

# **Tensile and Compressive Mechanical Properties of Billet Pressed LX17-1 as a Function of Temperature and Strain Rate**

*S. Groves, B. Cunningham*

**January 26, 2000**

*U.S. Department of Energy*

Lawrence  
Livermore  
National  
Laboratory

## DISCLAIMER

This document was prepared as an account of work sponsored by an agency of the United States Government. Neither the United States Government nor the University of California nor any of their employees, makes any warranty, express or implied, or assumes any legal liability or responsibility for the accuracy, completeness, or usefulness of any information, apparatus, product, or process disclosed, or represents that its use would not infringe privately owned rights. Reference herein to any specific commercial product, process, or service by trade name, trademark, manufacturer, or otherwise, does not necessarily constitute or imply its endorsement, recommendation, or favoring by the United States Government or the University of California. The views and opinions of authors expressed herein do not necessarily state or reflect those of the United States Government or the University of California, and shall not be used for advertising or product endorsement purposes.

This work was performed under the auspices of the U. S. Department of Energy by the University of California, Lawrence Livermore National Laboratory under Contract No. W-7405-Eng-48.

This report has been reproduced directly from the best available copy.

Available electronically at <http://www.doe.gov/bridge>

Available for a processing fee to U.S. Department of Energy  
and its contractors in paper from  
U.S. Department of Energy  
Office of Scientific and Technical Information  
P.O. Box 62  
Oak Ridge, TN 37831-0062  
Telephone: (865) 576-8401  
Facsimile: (865) 576-5728  
E-mail: [reports@adonis.osti.gov](mailto:reports@adonis.osti.gov)

Available for the sale to the public from  
U.S. Department of Commerce  
National Technical Information Service  
5285 Port Royal Road  
Springfield, VA 22161  
Telephone: (800) 553-6847  
Facsimile: (703) 605-6900  
E-mail: [orders@ntis.fedworld.gov](mailto:orders@ntis.fedworld.gov)  
Online ordering: <http://www.ntis.gov/ordering.htm>

OR

Lawrence Livermore National Laboratory  
Technical Information Department's Digital Library  
<http://www.llnl.gov/tid/Library.html>

**Tensile and Compressive Mechanical Properties of Billet  
Pressed LX17-1 as a Function of Temperature and Strain Rate**

**Scott Groves  
Bruce Cunningham**

**January 26, 2000**

Work performed under auspices of the U.S. Department of Energy by the Lawrence  
Livermore National Laboratory under contract No. W-7405-ENG-48

## **Introduction**

This report documents mechanical property test data on LX17-1, a plastic bonded explosive. The data was generated using equipment and test facilities situated at the High Explosives Test Facility (HEAF), Lawrence Livermore National Laboratory, Livermore, California. The report contains uniaxial tensile and compressive stress-strain data derived from tests performed at several temperatures and strain-rates. In addition, the report contains a number of scanning electron microscope images that show some of the structural aspects of the subject material.

## **A Description of the Material Tested**

All data reported herein was derived from tests performed on billet pressed LX17-1, a plastic bonded explosive composed of 92.5 %wt. wet aminated TATB (triamotrinobenzene) and 7.5 %wt. KEL-F 800, a chlorotrifluoroethylene/ vinylidene fluoride copolymer binder. In formulation, the constituents were initially mixed at elevated temperature to form a uniform blend of explosive and binder. Through careful control of temperature plus the addition of cooling water at the appropriate time in the process, small beads, referred to as molding powder beads, were formed. These beads, which are typically 500 to 1000 microns in size, were subsequently isostatically pressed at elevated temperature to form billets. These billets were then machined into test specimens.

Specifically, all tests were performed using specimens formed from molding powder (LLNL reference Serial # C 063) that was supplied by Mason and Hanger and produced by Holsten (MFG Lot # HOL 87H 851-01) in August, 1987. The powder was pressed into billets in May of 1998 and subsequently machined into test specimens. Figure 1 shows examples of machined tensile and compressive test specimens of the type tested. These specimens were produced by initially coring blanks from the billet, and subsequently lathe turning them to exact size.

Figures 2 and 3 show Scanning Electron Microscope (SEM) images of TATB crystals of the type used in formulating the material. Figure 4 is a plot showing particle size distribution for this material. Note the relatively complex structure of the larger particles, which consist of many tightly clustered and bound sub-particles. Figure 5 shows a bead of pure KEL-F 800. During molding powder formation, this material, which has a low

melting point (batch dependent, but typically between 60 and 100 degrees C), becomes liquid and uniformly coats the TATB crystals. Figure 6 shows an image of a molding powder bead in which TATB and KEL-F 800 binder have been combined but not pressed. Figure 7 is a view inside a bead showing the KEL-F-coated TATB crystals.

Once the TATB and KEL-F 800 have been combined, it is extremely difficult to visually assess the state of the TATB particles, which have experienced considerable mechanical trauma during mixing and pressing. To determine the end state of the crystals and the degree to which they may have been broken up during processing, acetone was used to dissolve away the binder from the pressed LX17-1. Images of crystals with binder removed are seen in Figures 8 and 9. In these images it can be seen that many large, complex crystals are still in evidence. However, it does appear that there has been some overall reduction in average particle size.

Figures 10 and 11 show SEM images of the machined surface of a compression specimen. Lathe tool marks are clearly visible and it appears that burnishing has taken place, possibly due to localized heating and melting of the binder as a result of friction.

Figures 12, 13, and 14 show views of an LX17-1 fragment that had been potted in epoxy and lapped using a series of successively smaller abrasive grits. In an effort to prevent the KEL-F from smearing, the sample was kept chilled and lapping was performed with a slurry of abrasive and ice water. In many cases, the dark spots are probably small voids caused when small TATB particles were dislodged from the surface during polishing. In other cases, dark regions appear to be actual voids present within TATB crystals (see Figure 14).

Figure 15 shows a post-test failure surface from a compression sample which was cold-tested at  $-50^{\circ}\text{C}$ . Surface features appear sharp and jagged and it is difficult to distinguish TATB from binder. This suggests that, when cold, the KEL-F is relatively strong and brittle, and therefore failure tends to occur across plains intersecting both crystals and binder. In contrast, Figure 16 shows a post-test failure surface from a compression sample tested at  $200^{\circ}\text{C}$ . Here, much of the surface is comprised of rounded features that look to be un-fractured TATB. Light colored, wispy regions are likely sheets of binder, pulled away from the TATB crystal surfaces.

## **The Mechanical Properties Test Equipment and Instrumentation**

The data presented here was generated using two MTS hydraulic tensile/compressive test frames situated at the Mechanical properties test laboratory, HEAF building, LLNL (see Figure 17). Each frame is independently computer controlled and capable of performing uniaxial tests at temperatures from below  $-50^{\circ}\text{C}$  to above  $200^{\circ}\text{C}$ . To date, tests have been performed at strain rates ranging from a relatively low  $4.0\text{e-}7$  in/in/s to above 1 in/in/s. Testing is performed inside closed, temperature-controlled ovens. For purposes of safety, and to allow testing to take place within inert gas atmospheres, specimens are secondarily contained within closed cylindrical canisters – see Figures 18 and 19. Elevated and reduced temperature tests were performed in helium atmospheres. Strain measurement was achieved using extensometers. The devices used include both commercially manufactured MTS units and also specially designed and fabricated LLNL multi-gage devices with built-in compensation for sample bending. For a detailed description of these devices, as well as a discussion of issues relating to mechanical properties testing of PBX materials see *Mechanical Testing of Plastic Bonded Explosives*, Groves, Cunningham, 1999 UCRL-ID-135245.

### **LX17-1 Mechanical Properties Data – General Remarks**

The data is shown in the form of stress-strain plots, both tensile and compressive, as well as in summary plots of ultimate strengths, initial moduli, and, in the case of tensile data, ultimate strains. The stress-strain plots are grouped in sets, both by constant temperature and constant strain-rate. Strain-rates range from  $4\text{e-}7$  in/in/s to over 1 in/in/s. Test temperatures range from  $-50^{\circ}\text{C}$  up to  $+125^{\circ}\text{C}$  in tension, and to as high as  $+220^{\circ}\text{C}$  in compression.

Individual stress-strain plots shown are, with few exceptions, actual data plots, and not fits, so that the exact character of the recorded stress-strain relationships is preserved. Exceptions occur where rapid ramp up to a high strain rate resulted in initial oscillatory behavior, a consequence of the equipment's inability to smoothly arrive at the target rate in the short time available.

In some cases, high-frequency, low-amplitude noise may be seen on portions of the curves. The noise, which effects only a minority of the curves, and generally only a portion thereof, is not believed to have significantly affected the result.

In many cases, tests were repeated to insure confidence in the data. Where redundant tests were performed, results were averaged to arrive at the values used to construct the summary plots that appear in the end of the compressive and tensile data sections.

### **Compression Data**

Presented in both fixed temperature and fixed strain-rate plot groupings (see Figures 20 through 27), the data shows a clear ordering, with strength increasing as temperature decreases and as strain rate increases. Strain rates were controlled via feedback from the extensometer and were generally true and constant to within 1%. Exceptions occurred in the case of the highest rate tests, where actual rates were consistently higher than the target rate of 1 in/in/s. At these high rates, machine response is inadequate to achieve either a constant (throughout the test) or repeatable result and so high test-rates fluctuated from between 1 and approximately 5 in/in/s. In these cases, rates shown are derived from straight-line fits to the latter portions of the strain time data curves – see Figure 28.

Figure 29 shows a series of constant strain-rate plots showing ultimate compressive strengths as a function of temperature. The plots are very well ordered, with strengths decreasing between  $-50^{\circ}\text{C}$  and  $0^{\circ}$ , followed by a continued but even more accelerated drop between 0 and  $+50^{\circ}\text{C}$  (the glass transition temperature for KEL-F 800 is approximately  $28^{\circ}\text{C}$ ). Finally – based on limited data - strength approaches zero above  $200^{\circ}\text{C}$ . Note that the exact melting point for KEL-F is heavily lot dependent, but generally occurs between 60 and  $100^{\circ}\text{C}$ . It is conjectured that this accounts for the comparatively constant indicated strength for the .0001 in/in/s strain-rate curve between 100 and  $200^{\circ}\text{C}$ . At these temperatures the binder should contribute very little to the strength of the material (except perhaps that it acts as a sticky paste to keep the TATB particles cohesive). Since TATB crystals maintain their strength well above  $200^{\circ}\text{C}$ , what strength the material does exhibit might be expected to result from irregular shaped TATB particles interlocking. Such a condition would suggest that measured strengths above  $100^{\circ}\text{C}$  might be expected to be somewhat inconstant, since

collapse would occur via a series of random localized failures (see Figure 30).

Figure 31 shows constant strain-rate plots of initial modulus values as a function of temperature. The plot values were determined by generating straight-line fits to the initial portion of the stress-strain curves between 200 and 1000 micro-strain. Data between 0 and 200 micro-strain was not included due to the fact that the first portion of the data curve is often compromised by “settling-in” phenomena that can occur as grips or platens first apply load to the specimen.

The initial modulus data is, with some exception, generally well ordered. The dominant trend is modulus decreasing with temperature and increasing with strain rate. As was the case for ultimate strengths, the greatest rate of change with temperature occurs between 0 and 50° C. Note that the high strain rate initial modulus values are particularly subject to error due to control instabilities during ramp-up.

An examination of the data shows that compression specimens of LX17-1 frequently sustain 50,000 microstrain (5% strain) or greater, prior to complete collapse. For this reason, ultimate compressive strain (strain to failure) is not a particularly useful measurement. An examination of strain to peak strength revealed no apparent ordering with either test temperature or strain-rate. However, for this data set, peak strength for all tests occurred between 15000 and 25000 microstrain (1.5 - 2.5% strain) with the average strain-to-peak-strength occurring at approximately 20,000 microstrain.

### **Tensile Data**

Figures 32-35 show LX17-1 fixed rate tensile plots at different temperatures. Figures 36-40 show fixed temperature plots at different rates. The data is generally well ordered with temperature and strain-rate. Exceptions are seen in Figures 33 and 34, which show stress-strain plots at different rates for temperatures of -20° C and 0° C respectively. Here strict ordering by rate is not sustained among some of the low rate tests. It is not known whether this is simply the result of statistical scatter, or is an indication of slight anomalies in material behavior at cold temperatures.

A summary graph of ultimate strengths in tension is shown in Figure 41. As was the case for similar compression data, ordering is very good, with slight

inconsistencies in low-temperature, low-rate data (see paragraph above). At the high temperature, strength would appear to approach zero above 100° C. This likely due to the fact that, at these temperatures, the melting point of KEL-F 800 has been exceeded and so there is little to hold the TATB crystals together under tensile loading.

Figure 42 shows initial modulus data for LX17-1 as a function of temperature and rate. Overall, the trend is as expected, with the modulus decreasing with temperature and increasing with rate. In detail, the curves indicate relatively small changes in modulus between -50 and 0° C, a rapid decrease in modulus as temperature increases from 0 to 50° C, and the initial modulus approaching 0 above 100° C. As was true with high rate compression, initial modulus values derived from high rate tension tests are subject to error due to control inadequacies during ramp-up (see Figure 40a, for example)

Finally, Figure 43 is a plot of ultimate tensile strains as a function of temperature and strain rate. The reader should be cautioned that ultimate tensile strain measurements are particularly subject to scatter due a tendency for stress concentrations in surface defects, such as machine marks, to induce premature failure. Keeping this in mind, it is interesting to note that all curves in Figure 43 initially show a slight decrease in ultimate strain between with increasing temperature, followed by sharp increase. Thereafter, low rate tests show a leveling off in maximum strain between 20 and 50° C.

## **Conclusions**

We have presented tensile and compressive data in detail and in summary for LX17-1, a plastic bonded explosive consisting of 92.5% wet aminated TATB and 7.5% KEL-F 800 binder. Generally, the data shows consistent ordering of strength and modulus, each of which generally decrease with increasing temperature and increase with increasing strain rate. These parameters show the greatest sensitivity to temperature change between 0° and 50° C, which is consistent with the fact that the glass transition temperature for LX17-1 is approximately 28° C. The data shows strengths approaching zero above 100° C in tension, and above 200° C in compression. Material behavior above 100° C is likely to be largely attributable to the low melting point of the binder.

# Figures

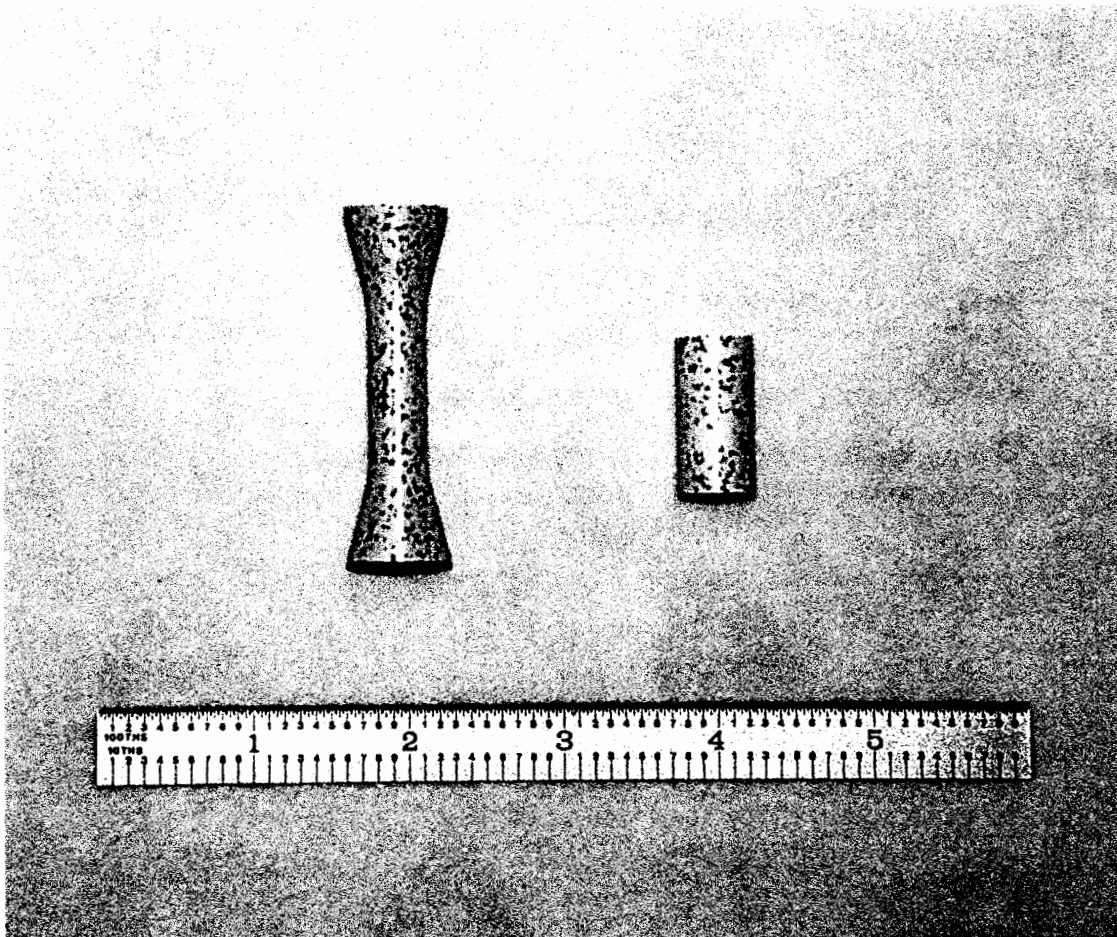


**Figure 1. LX17-1 tensile and compression test specimens. The scale shown is in inches.**

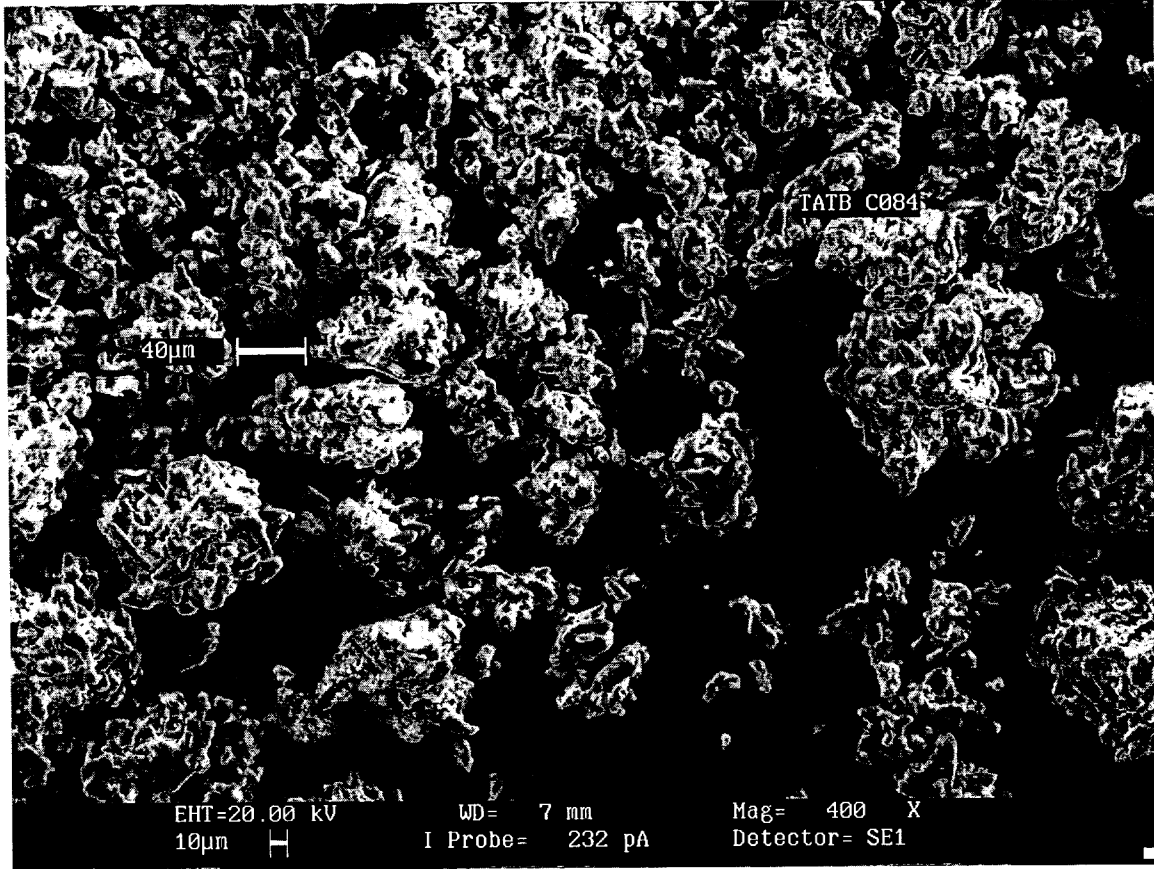


**Figure 2 – Wet aminated TATB crystals prior to combination with KEL-F 800 binder.**

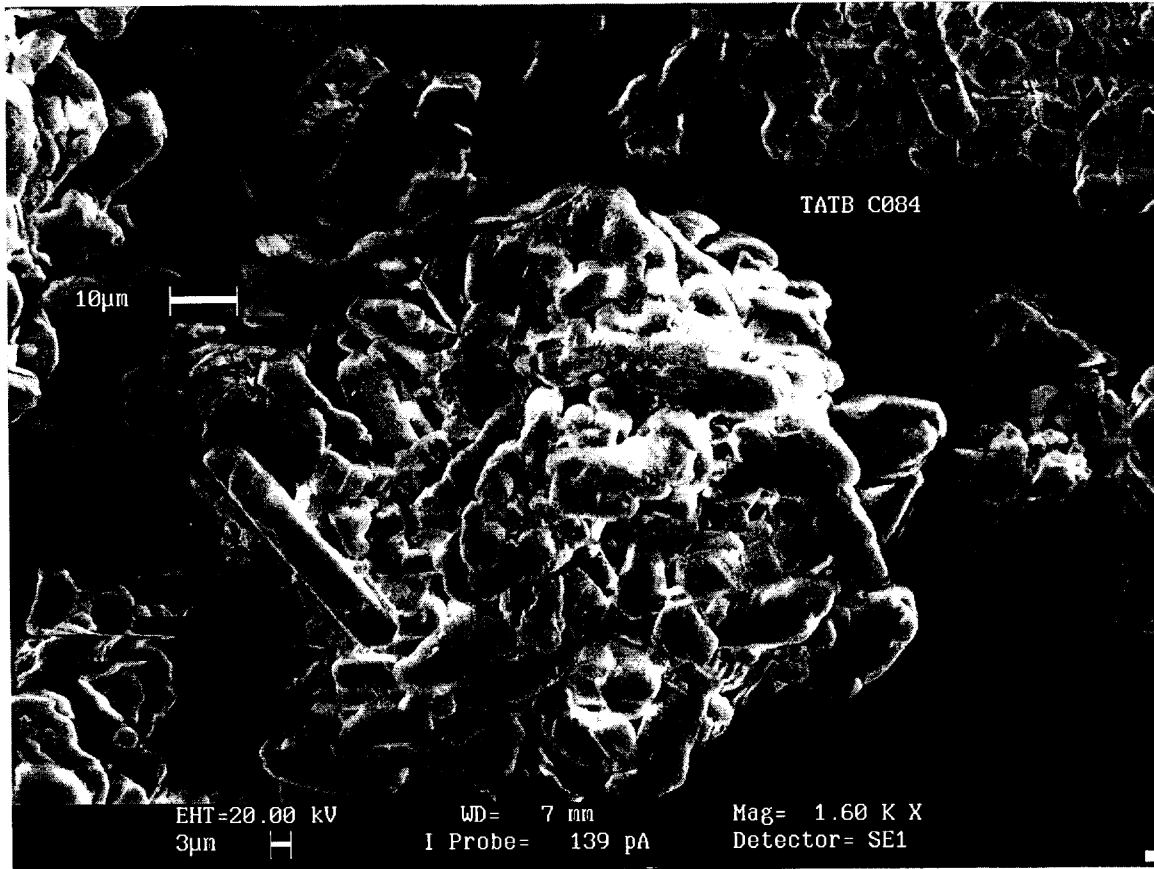


**Figure 3 – A single TATB particle approximately 100 microns across.  
Note the relatively complex structure.**

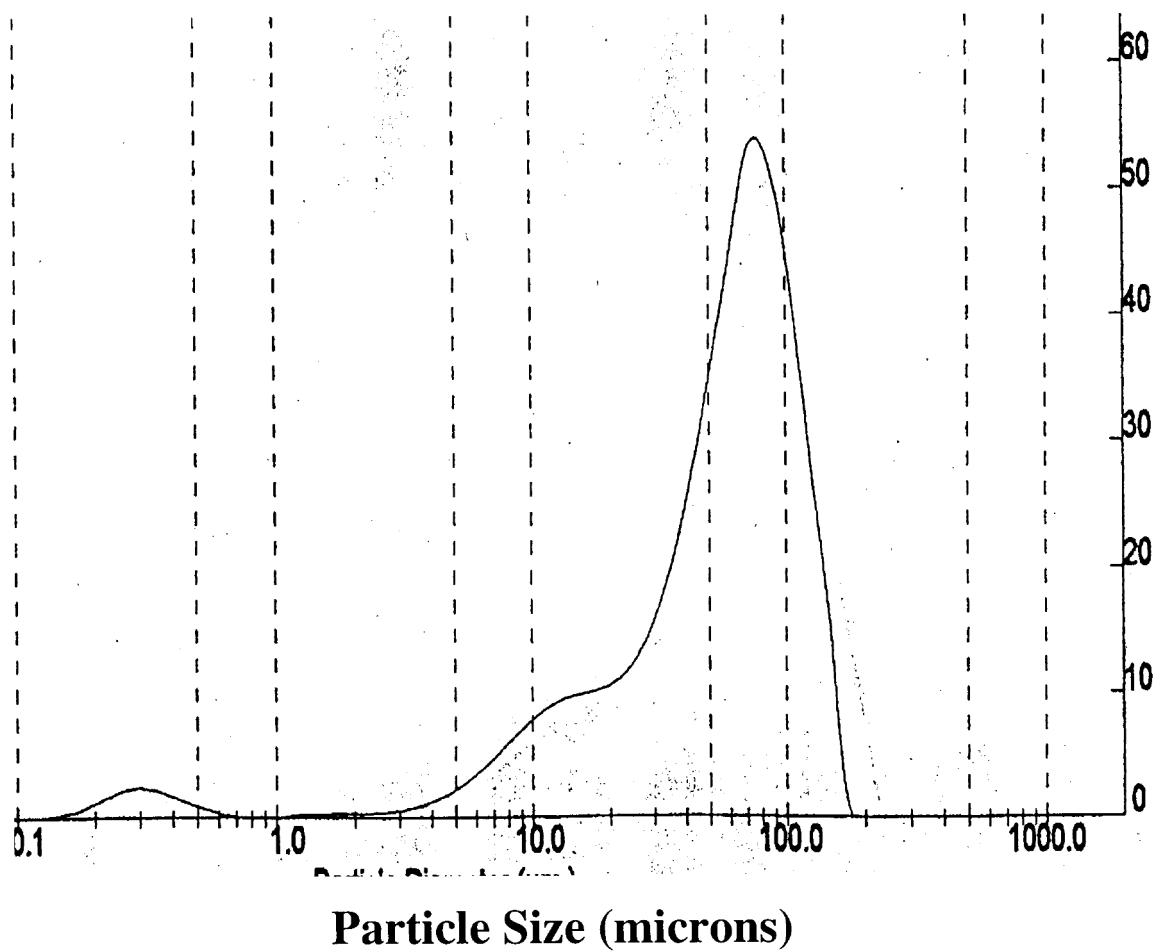


**Figure 4 – Relative particle size distribution of wet aminated TATB**

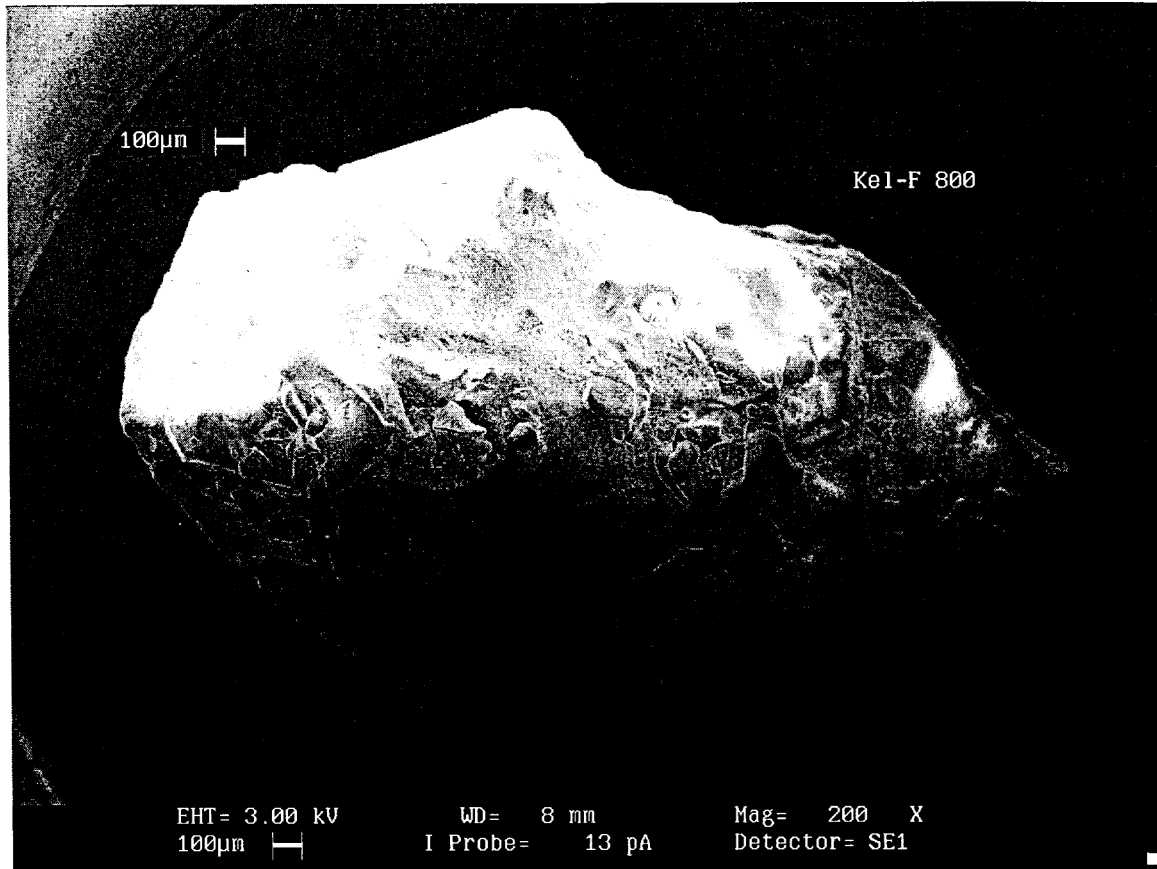


**Figure 5 – A bead of pure KEL-F 800 binder. This material has a melting point that is batch dependent but typically between 60° C and 100° C.**

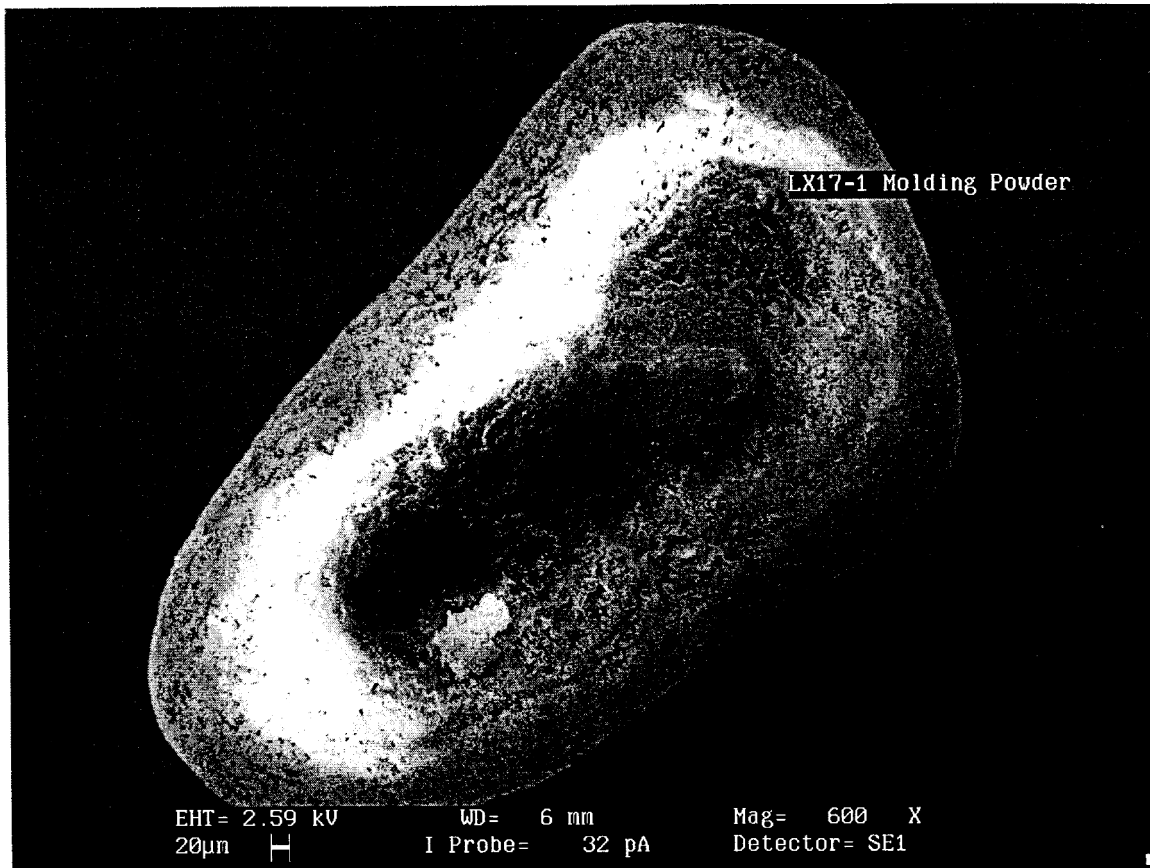


**Figure 6 – An LX17-1 molding powder bead. At this stage in the fabrication process, the energetic and binder have been combined but not yet pressed.**



**Figure 7 – Inside a molding powder bead showing TATB crystals coated with KEL-F 800.**

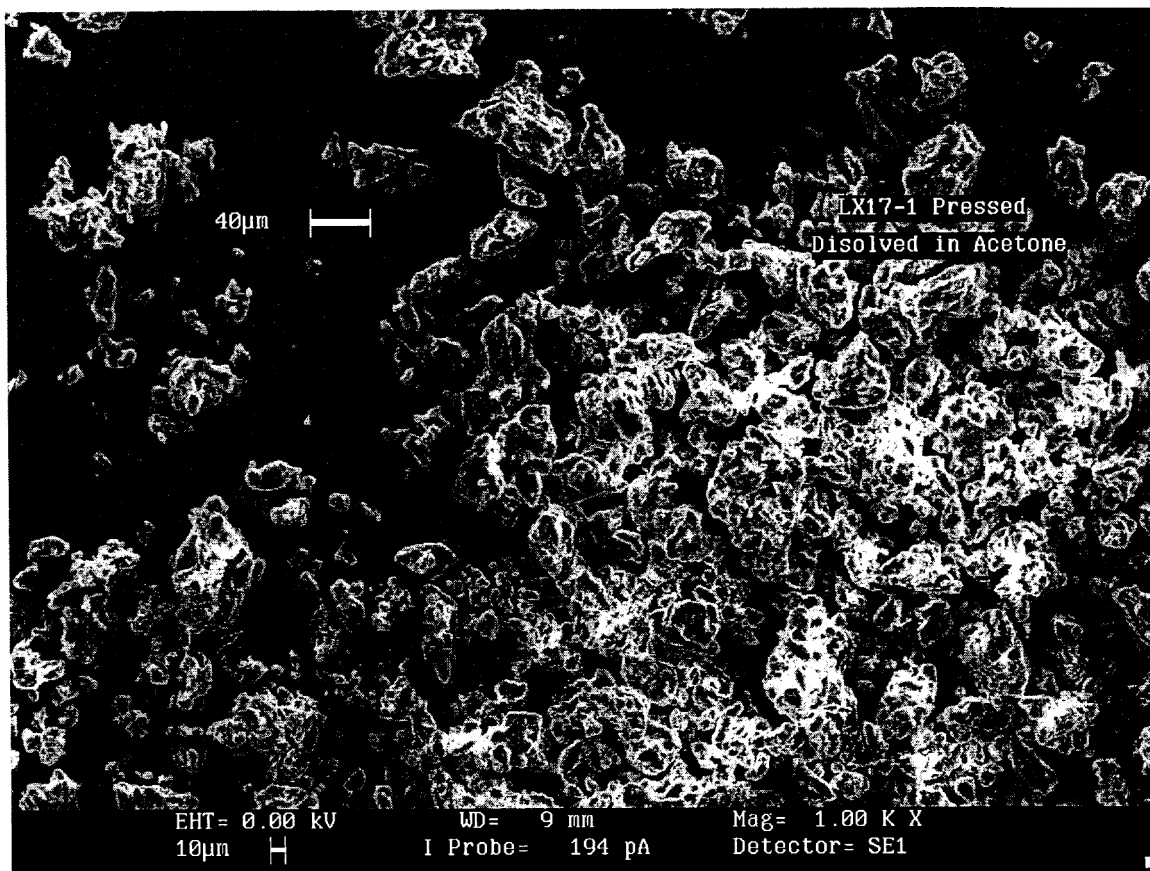


**Figure 8 – TATB crystals after the binder was removed from pressed LX17-1 by dissolving it in acetone.**

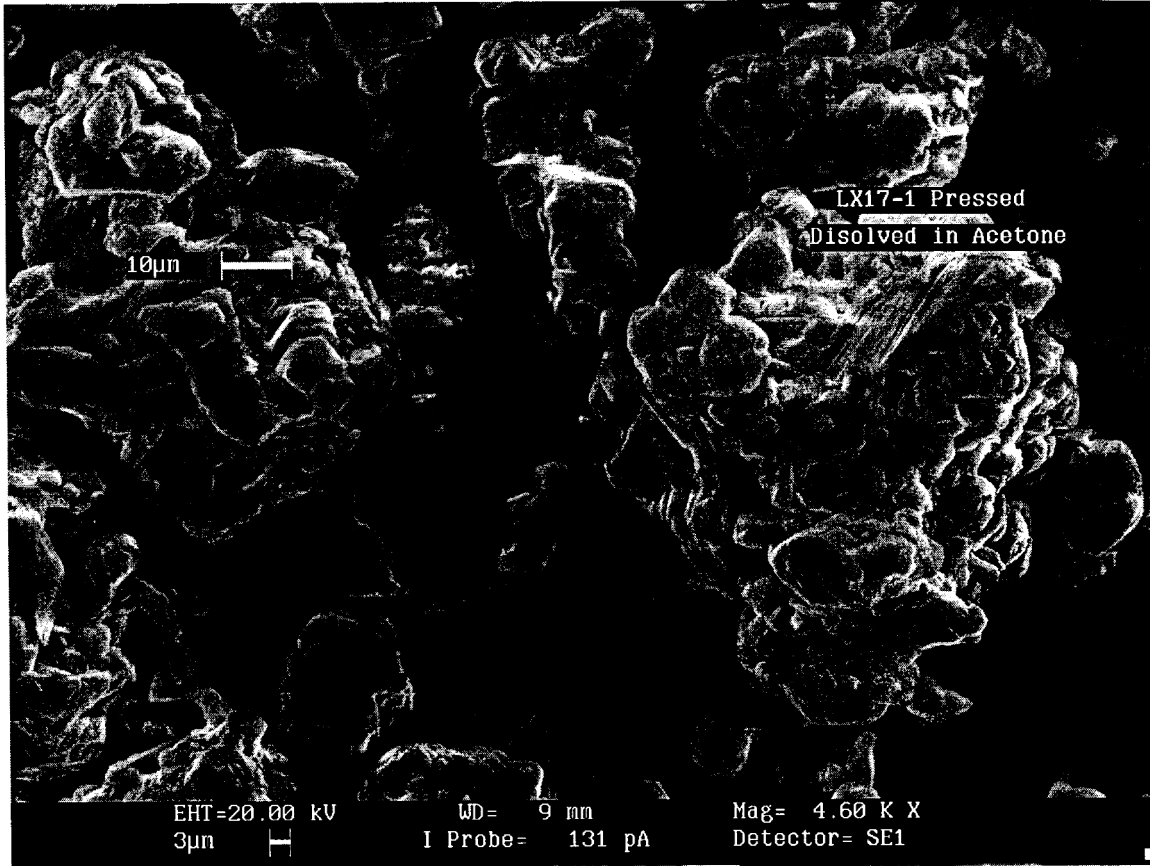


**Figure 9 – A higher magnification image of TATB crystals after the binder has been removed. Many of the particles are still large and complex, although the average particle size appears to have been reduced somewhat.**

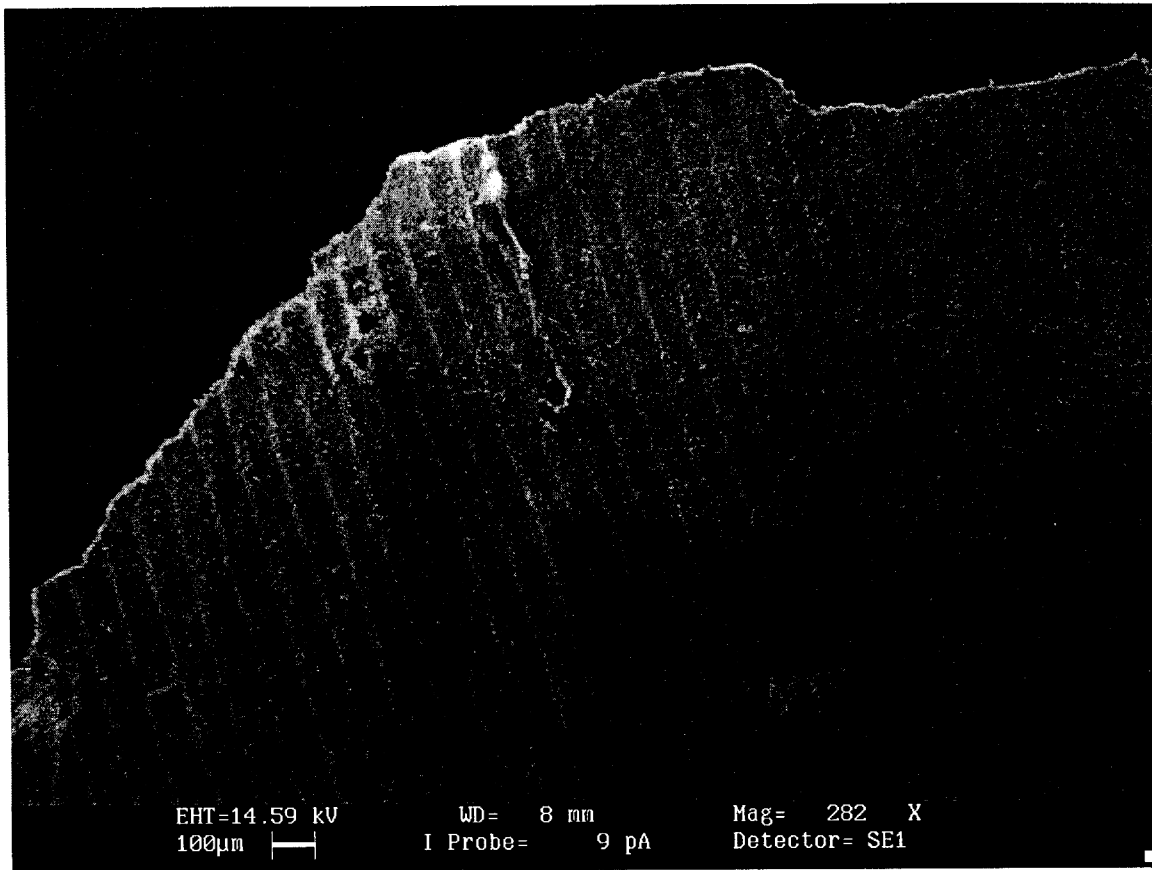


**Figure 10 – A flake from an LX17-1 compression sample showing the marks left on the outside surface by a lathe machine tool.**

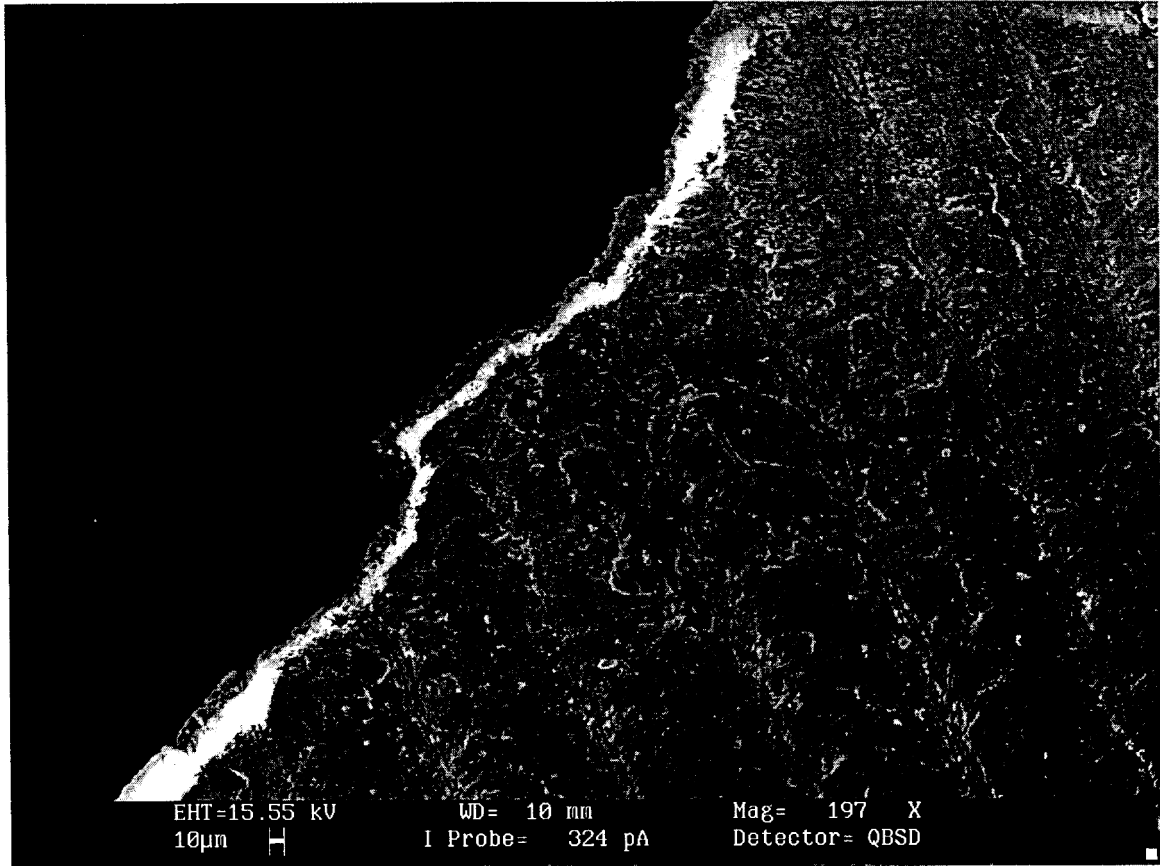


**Figure 11 – A higher magnification of the surface shown in Figure 10. Burnishing is suggested, possibly the result of friction-induced localized heating during the machining process.**

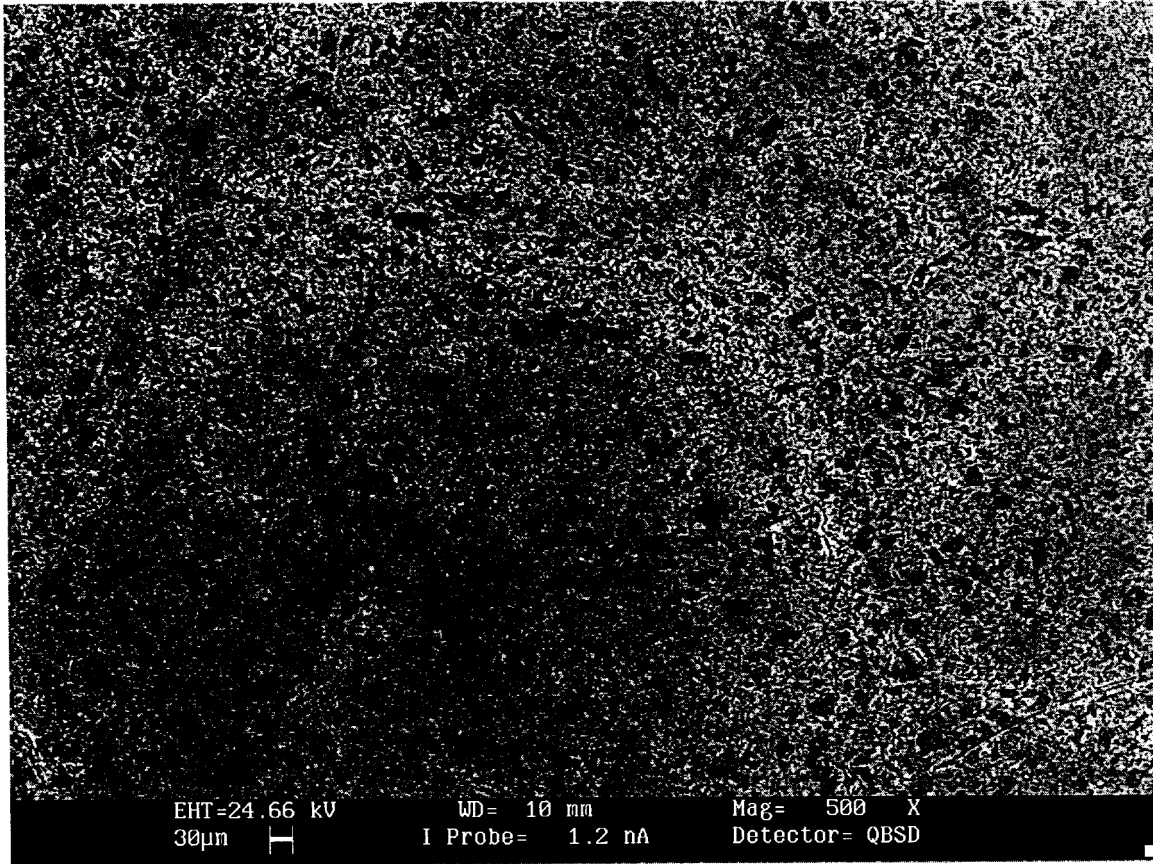


**Figure 12 – A low-magnification image of LX17-1 that was lapped at cold temperatures. The dark and light regions are crystal and binder.**

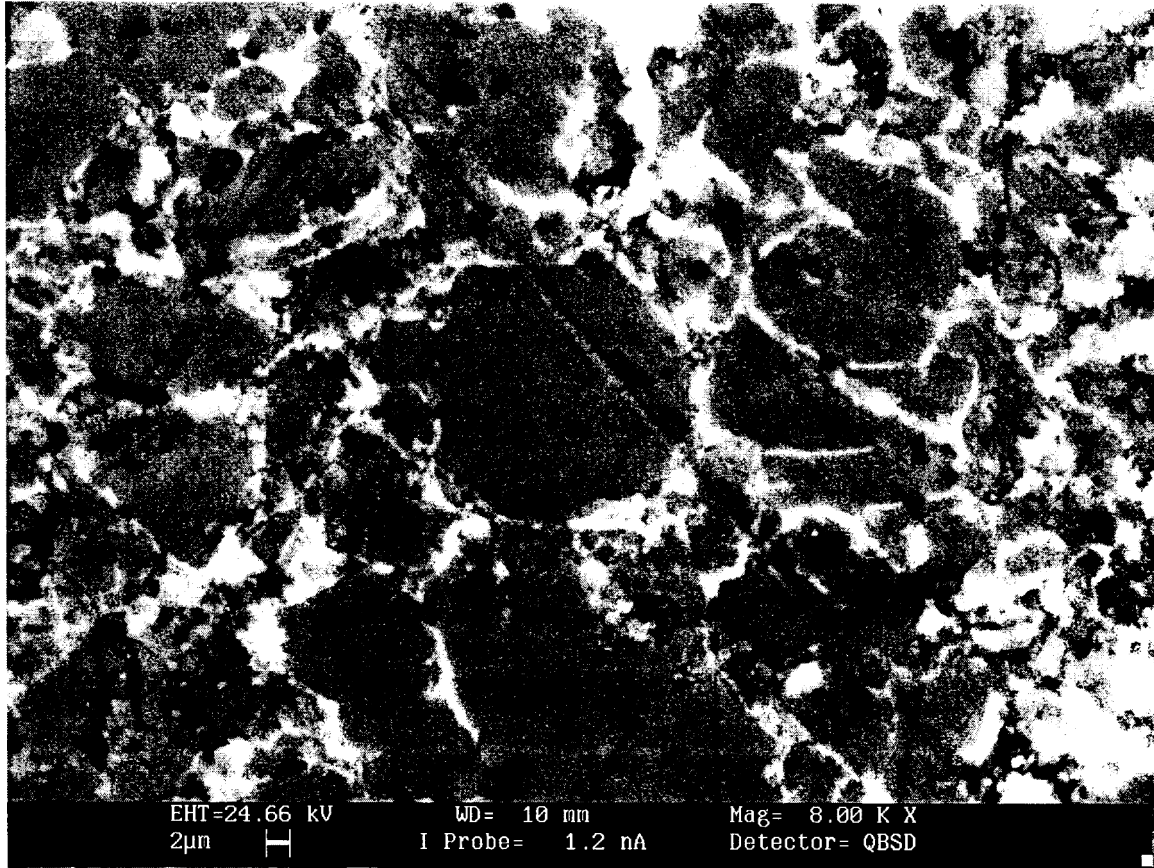


**Figure 13 – A higher magnification image of cold-lapped LX17-1. The prominent line is most probably a large-grit scratch mark which was not eliminated by subsequent smaller grit polishing.**

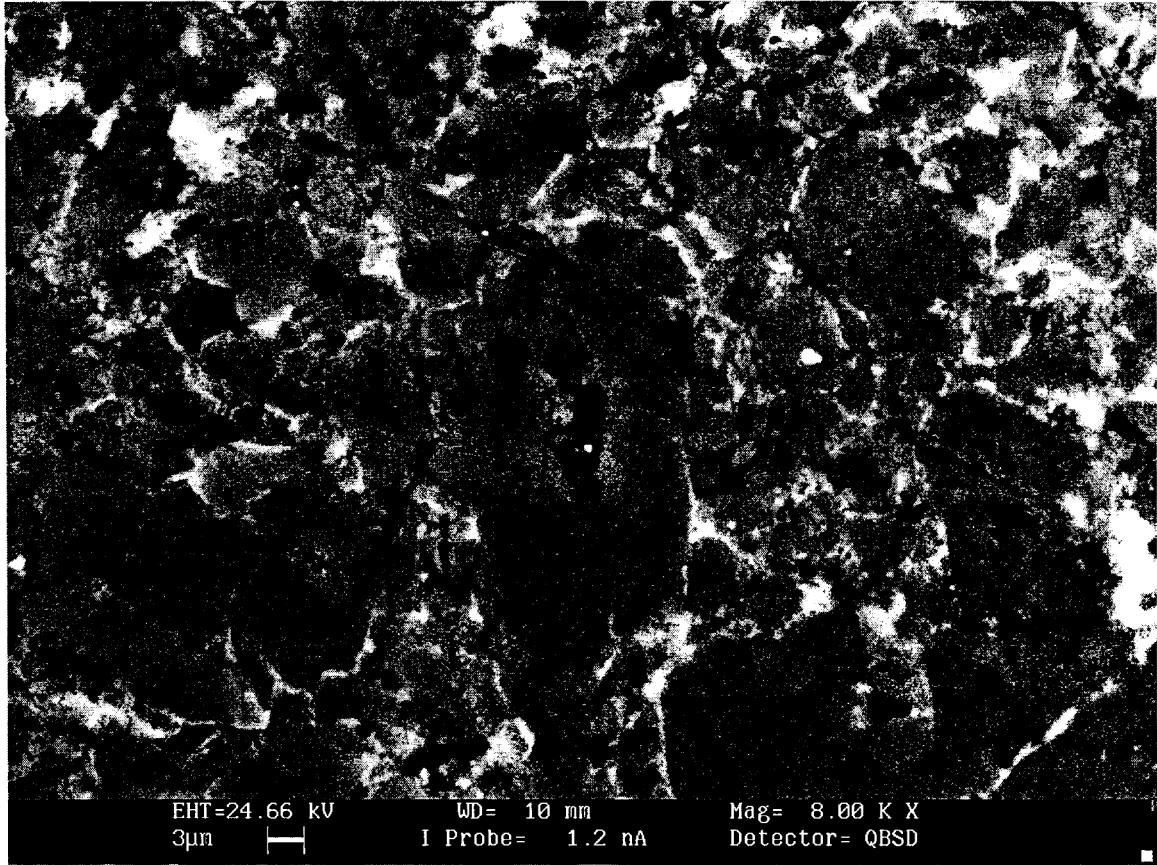


**Figure 14 – Lapped LX17-1. Some of the small white specks are probably lapping abrasive. Dark regions may be voids, in some cases the result of TATB particles being lifted from the surface during lapping. However, there also appear to be in-crystal voids (see, for example, the large dark area at the center of the image).**

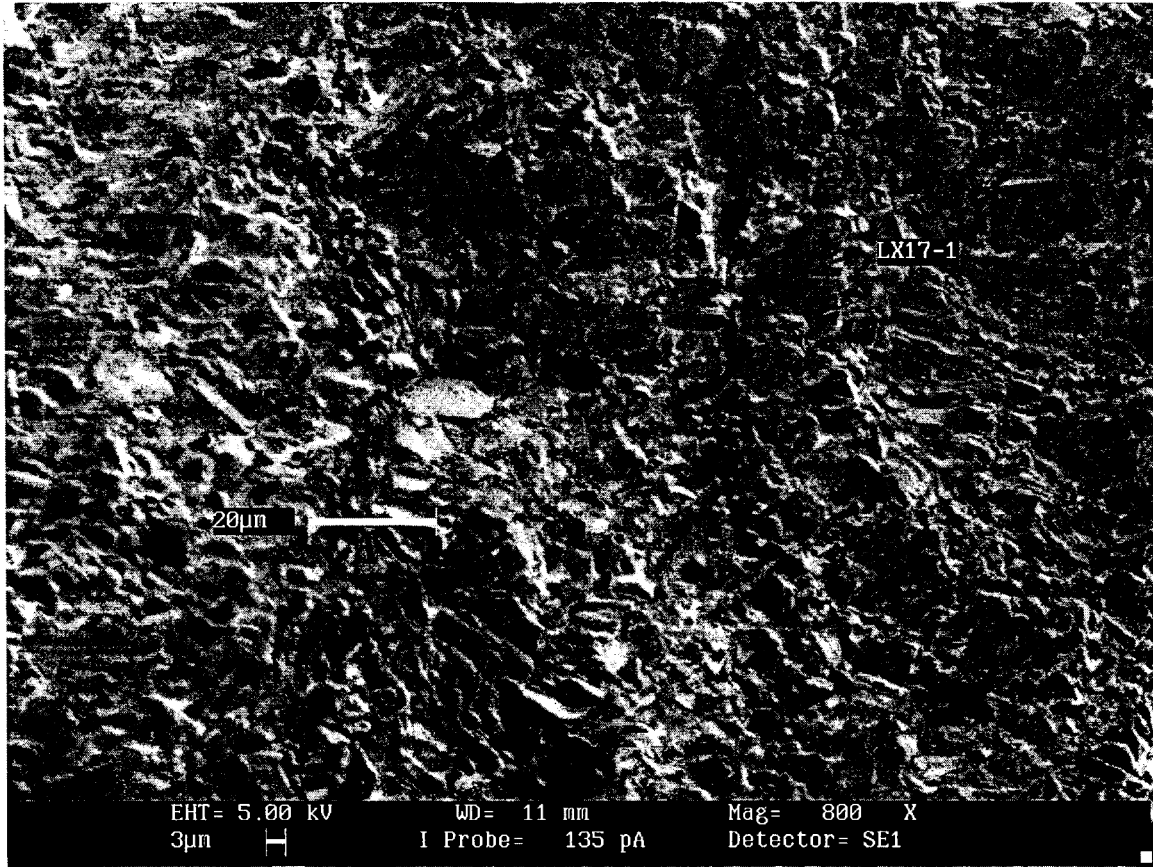


**Figure 15 – The fracture surface from a post-test compression sample tested at  $-50^{\circ}\text{C}$ . The surface appears to be jagged, suggesting fracture across both crystal and binder.**

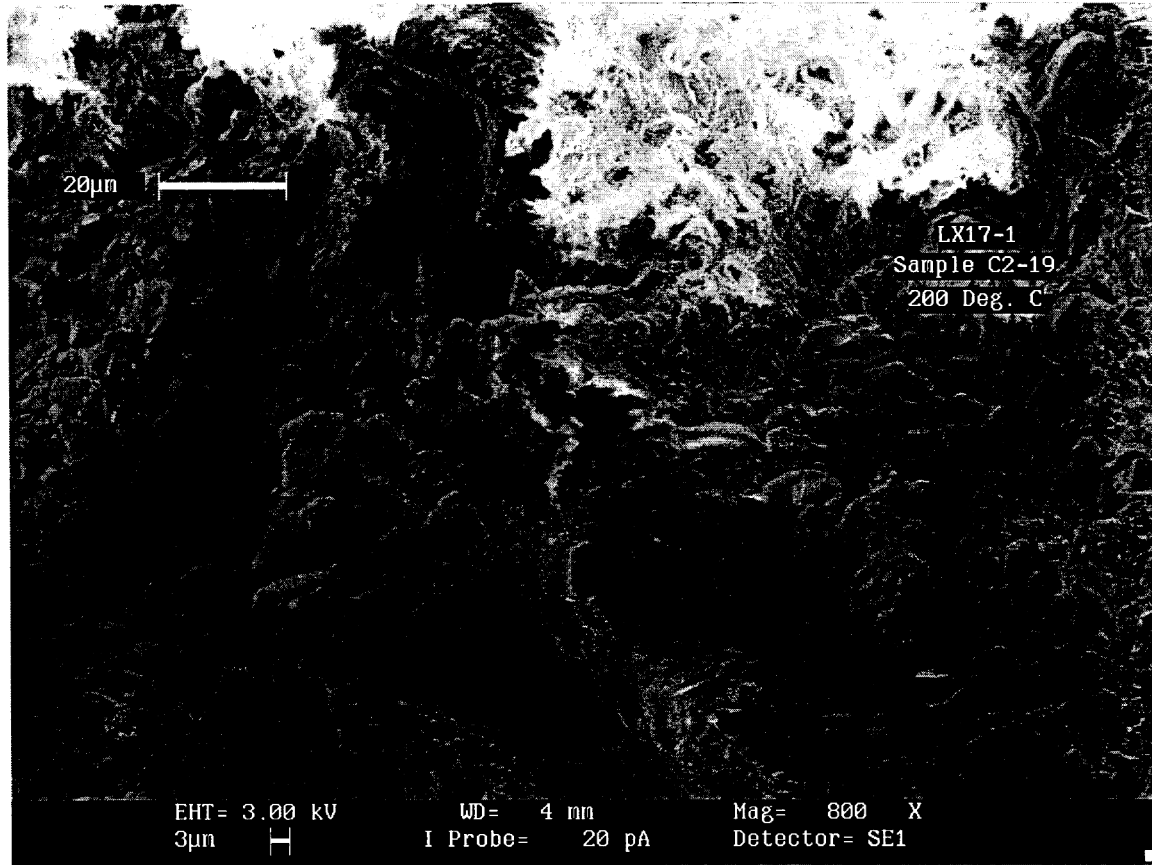


**Figure 16 – The fracture surface of a post-test compression sample tested at 200° C. Features appear rounder than in Figure 15, suggesting that the binder pulled away from the TATB crystals at failure. There also appears to be binder film (light areas) detached from the crystals.**

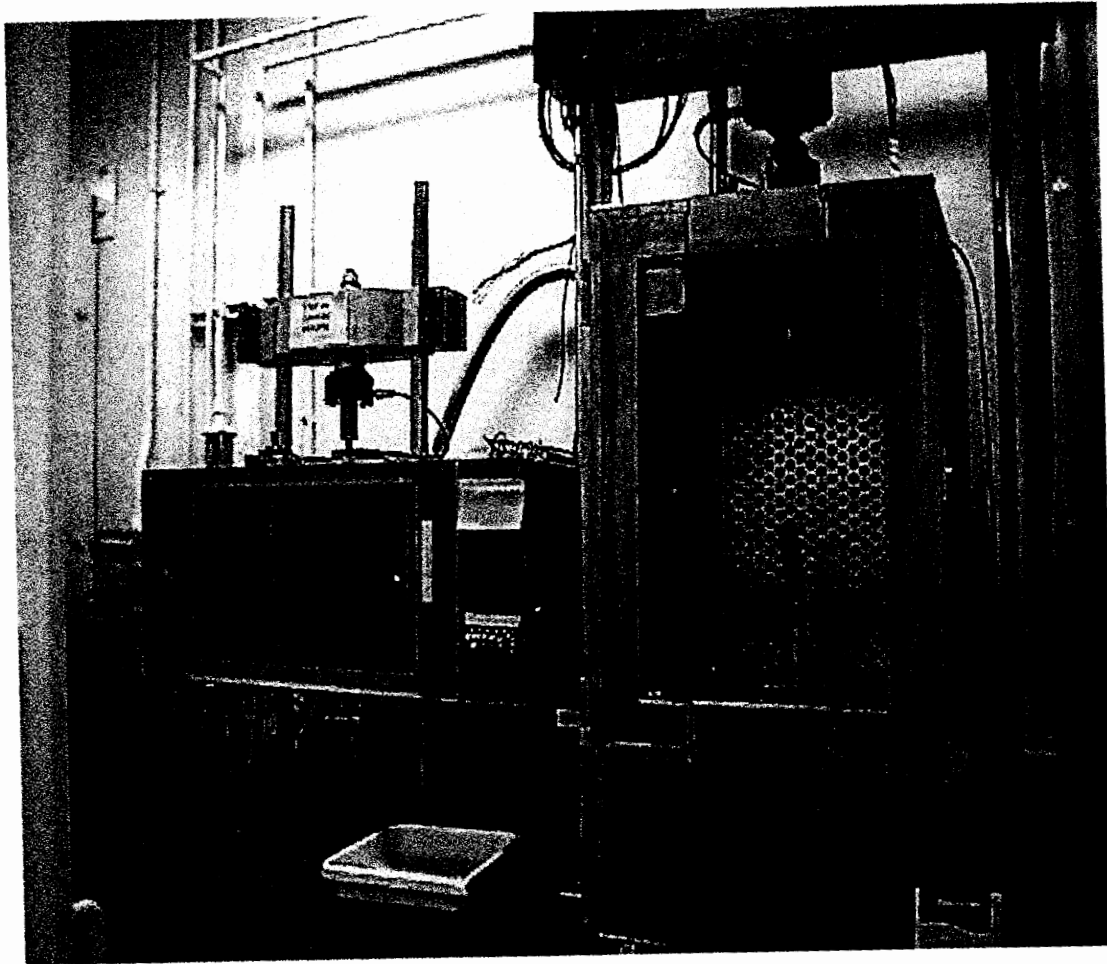


**Figure 17 – Computer controlled, hydraulically actuated tensile and compression MTS test machines with thermal enclosures (doors removed).**

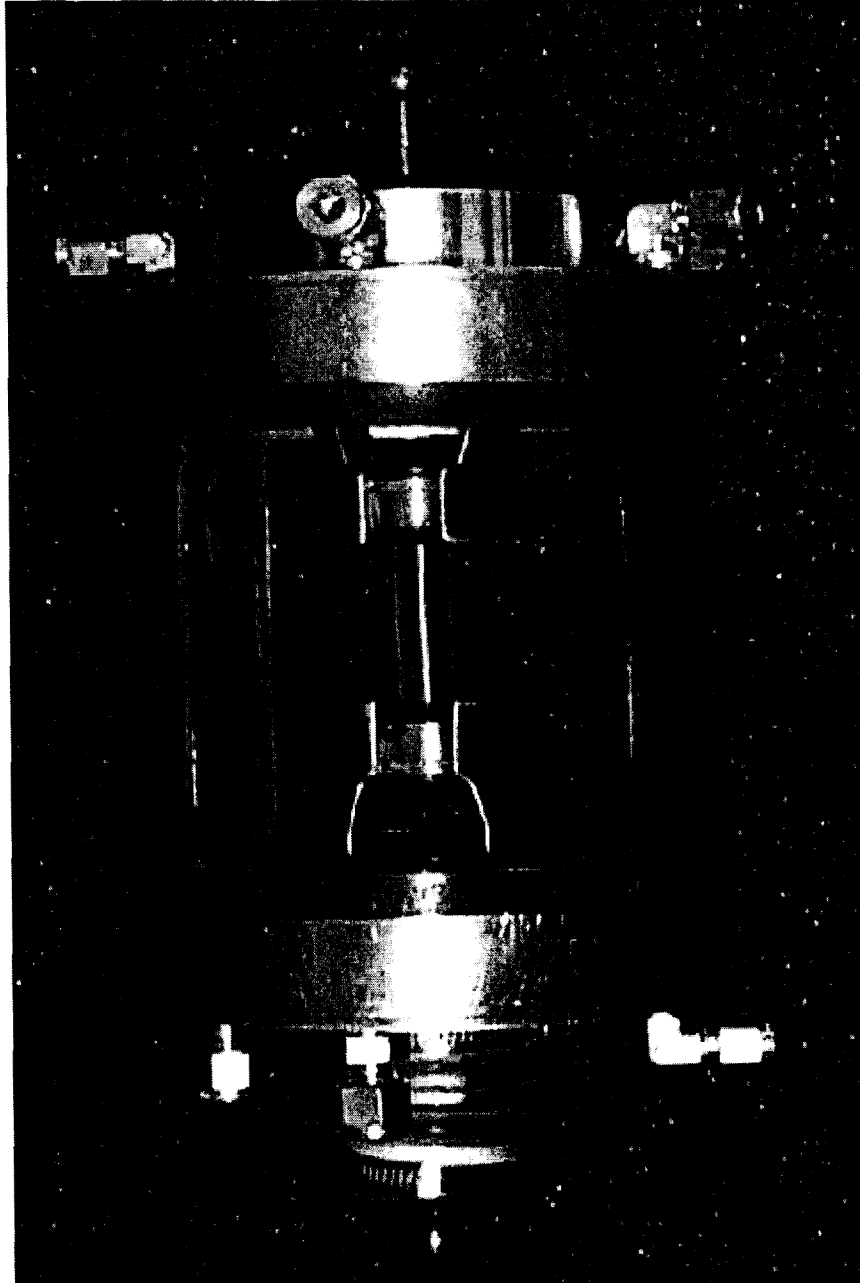
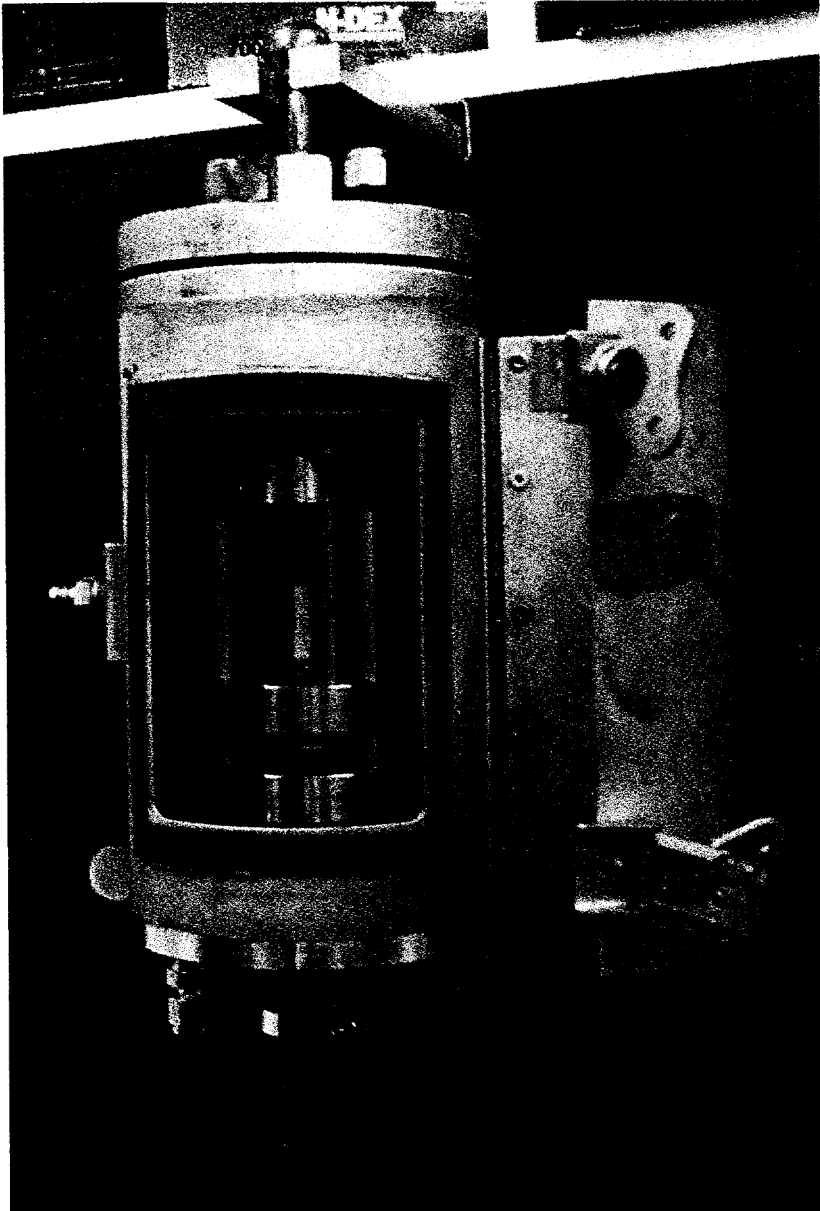


**Figure 18 – A tensile-test canister used to contain post-test debris, as well as inert gas, which flows around the specimen during elevated and reduced temperature tests. The covers have been removed to expose the grips and test sample.**



**19 – A compression canister showing the enclosed, very rigid compression fixture which is designed to actuate by pulling at each end.**

**LX17-1 Compression @ T=22° C**

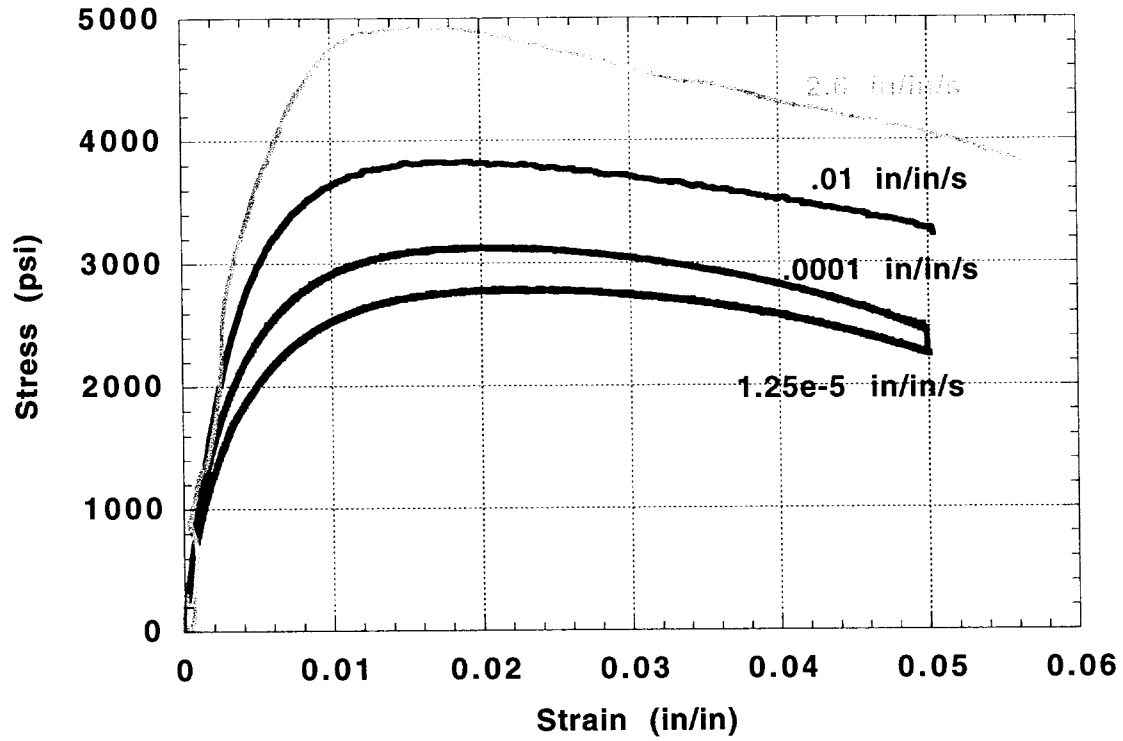


**Figure 20 – Stress-strain compression data at 22° C and four strain rates.**

LX17-1 Compression @ T=-50° C

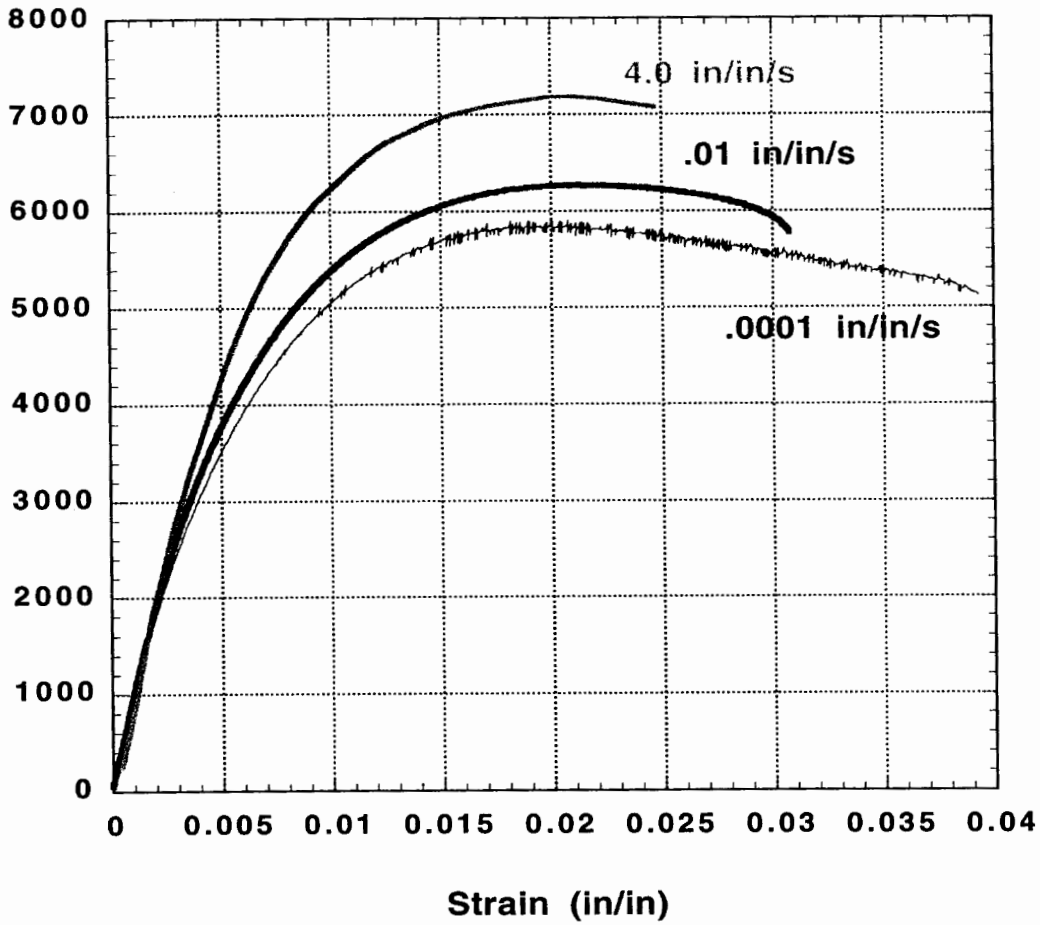


Figure 21 – Stress-strain compression data at -50° C and three strain rates.

LX17-1 Compression @ T=-12° C

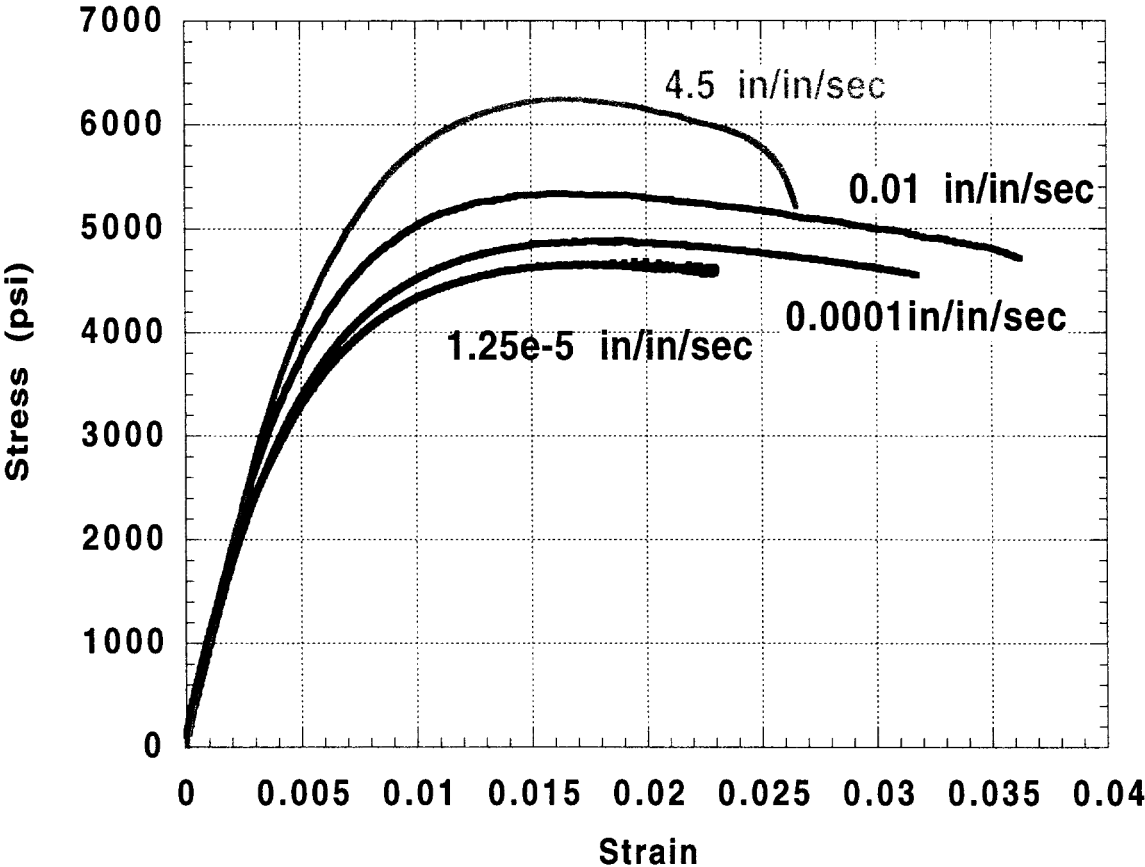
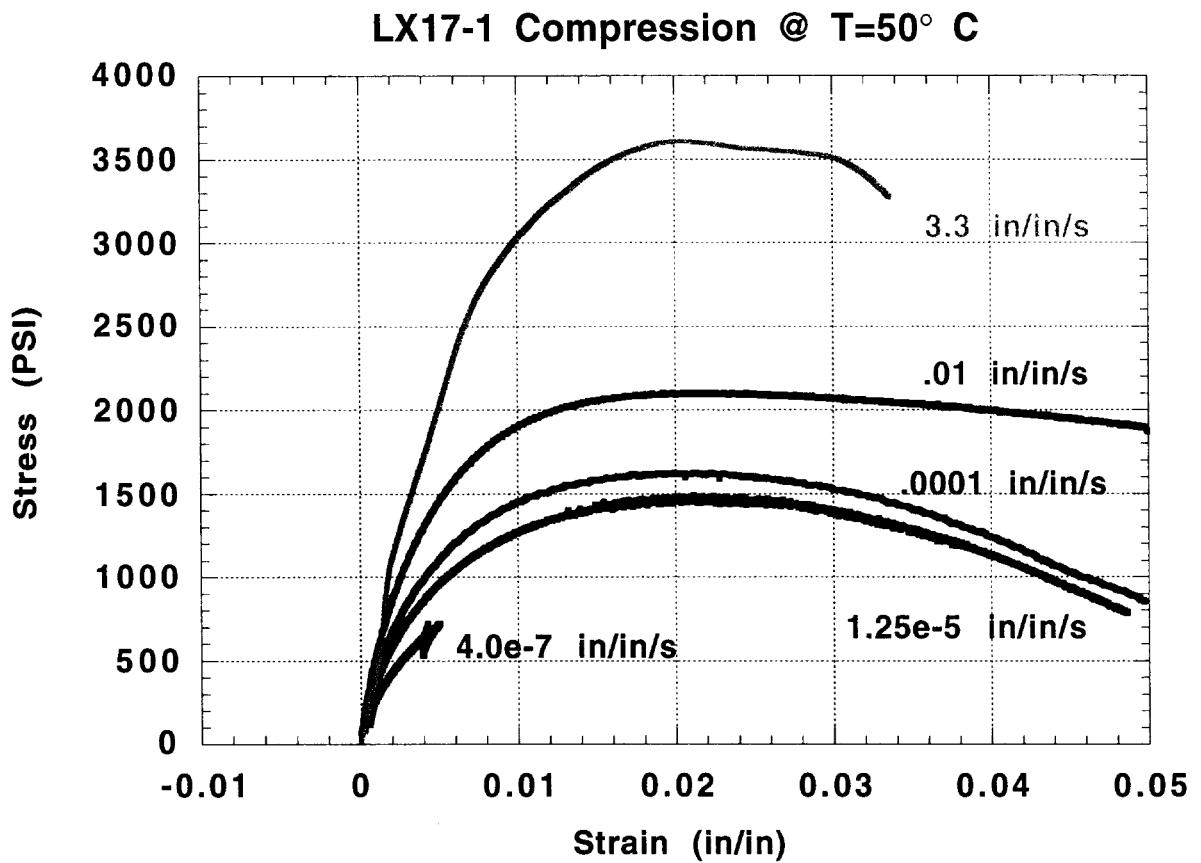
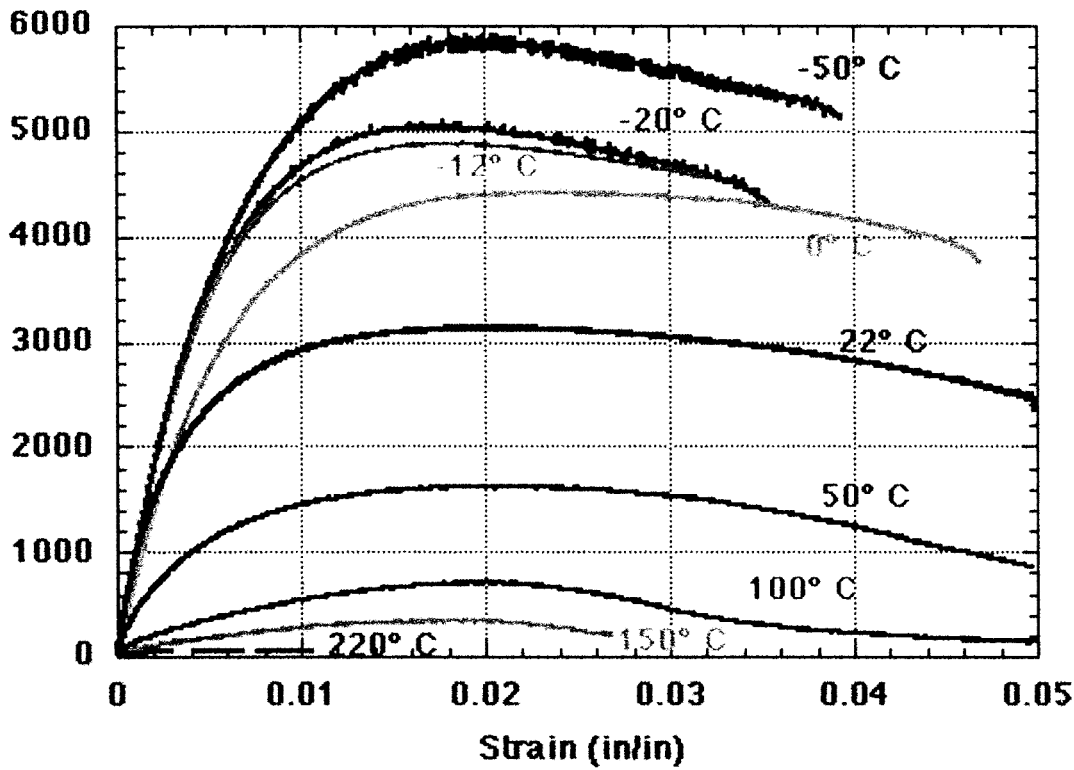


Figure 22 - Stress-strain compression data at -12° C and four strain rates.



**Figure 23 – Stress-strain compression data at 50° C and four strain rates. The low rate test at 4e-7 in/in/s was stopped at 50,000 microstrain.**

LX17-1 Compression @ SR=.0001 in/in/s



re 24 – Stress-strain compression data at strain rate = .0001 in/in/s and nine temperatures.

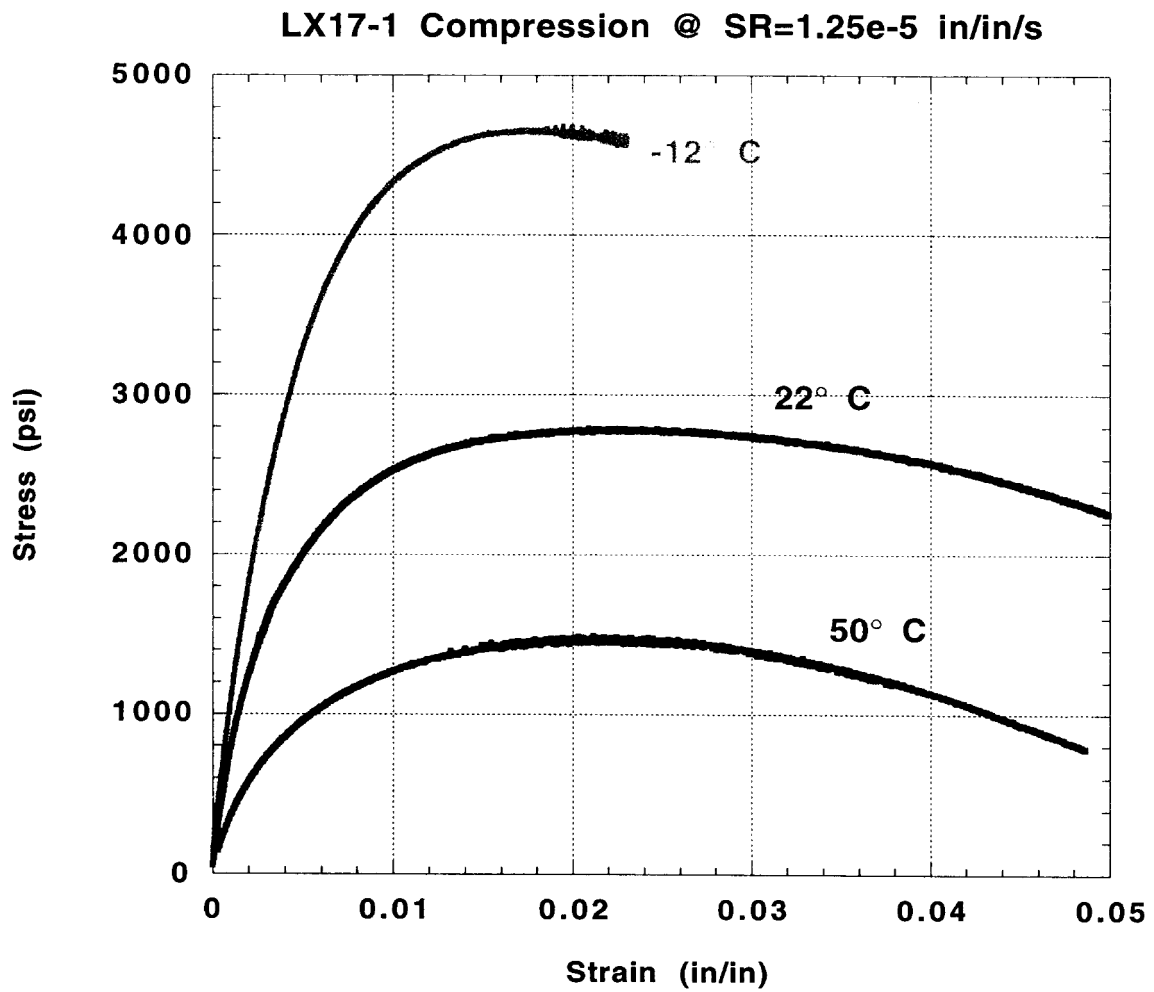
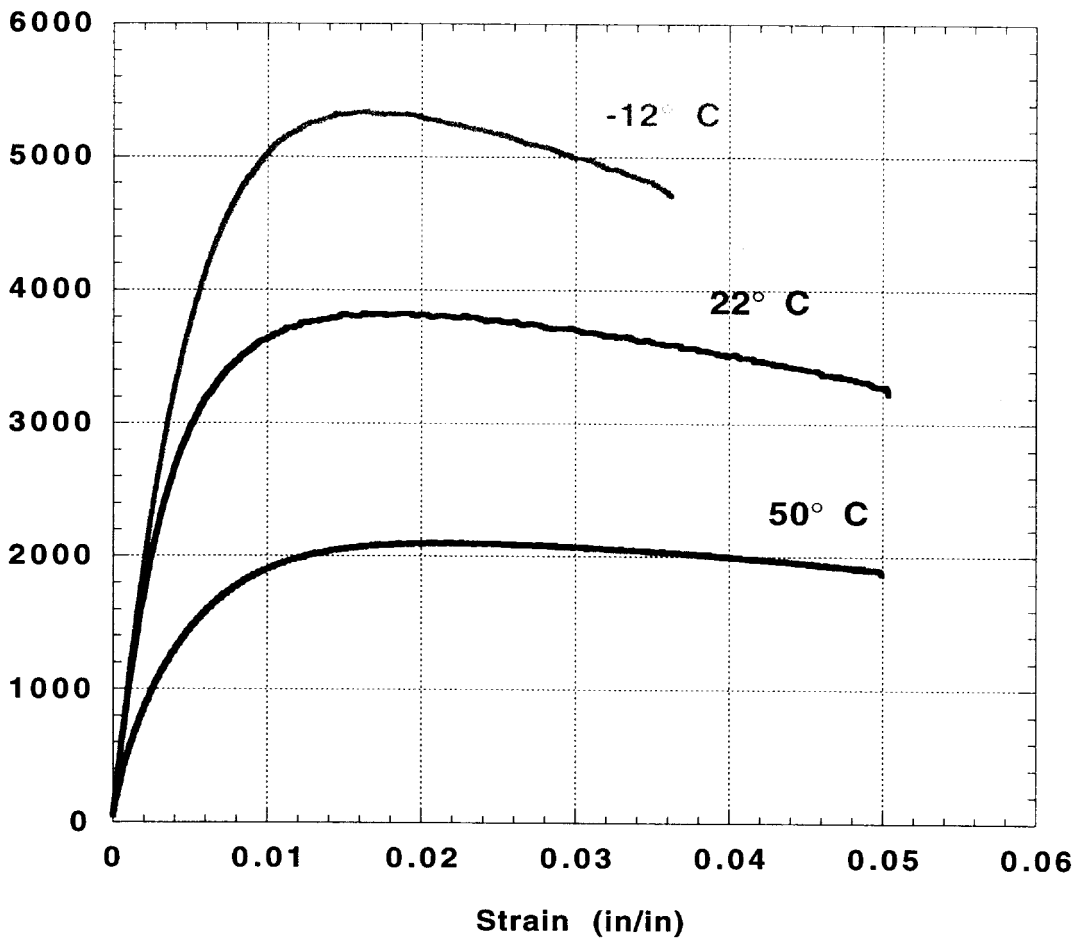


**Figure 25 – Stress-strain compression data at strain rate = 1.25e-5 in/in/s and three temperatures.**

**LX17-1 Compression @ SR=.01 in/in/s**



**re 26 – Stress-strain compression data at strain rate = .01 in/in/s and three temperatures.**

**LX17-1 Compression @ Ave. SR >1.0 in/in/s**

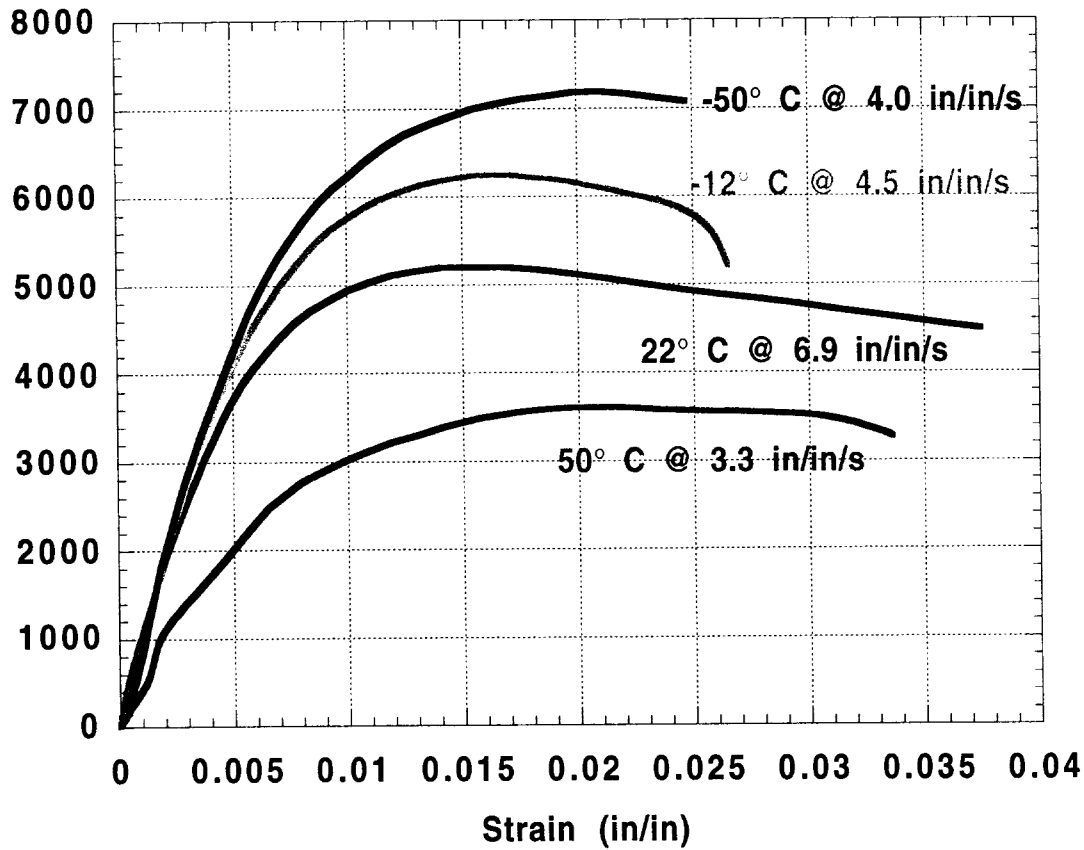


**Figure 27 – Stress-strain compression data at strain rates greater than 1.0 in/in/s and four temperatures.**

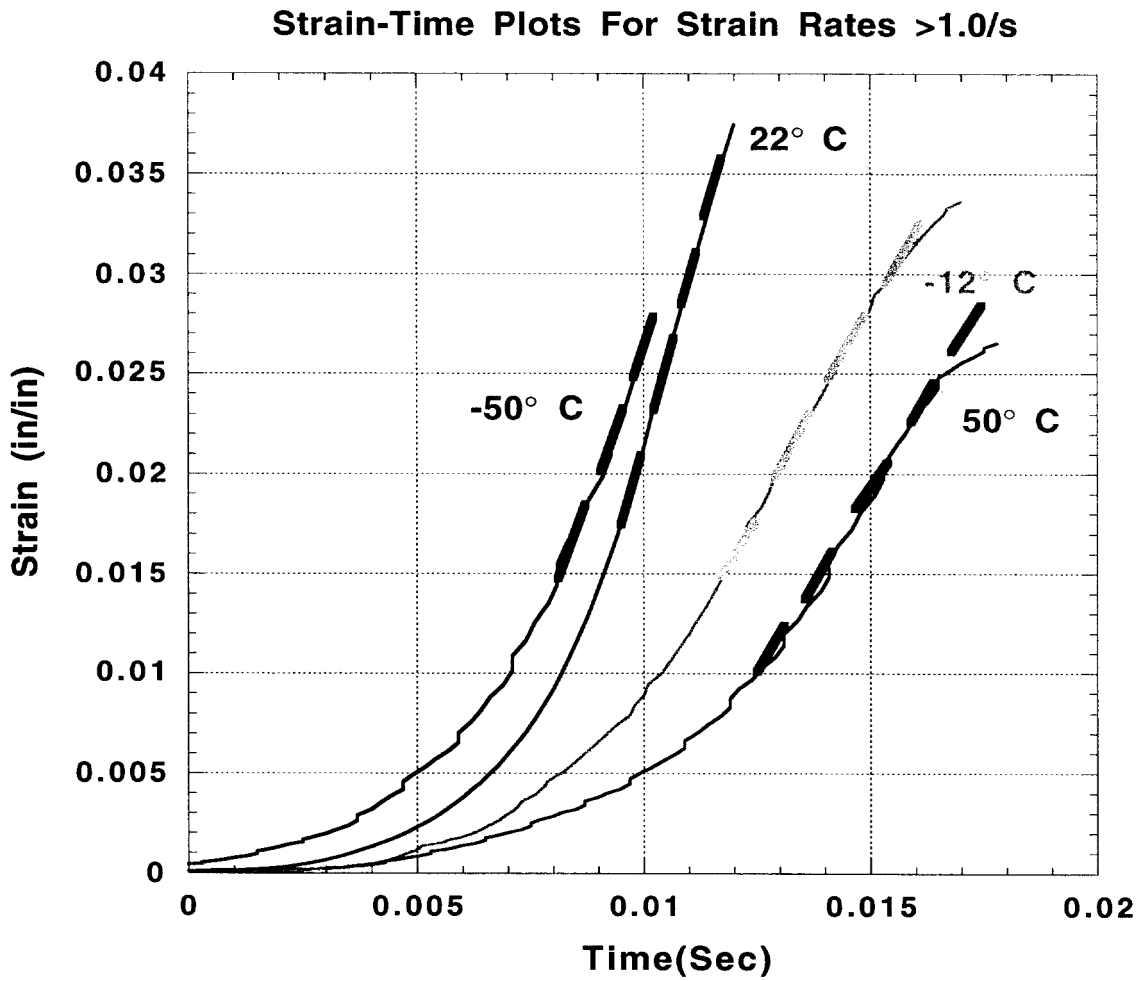
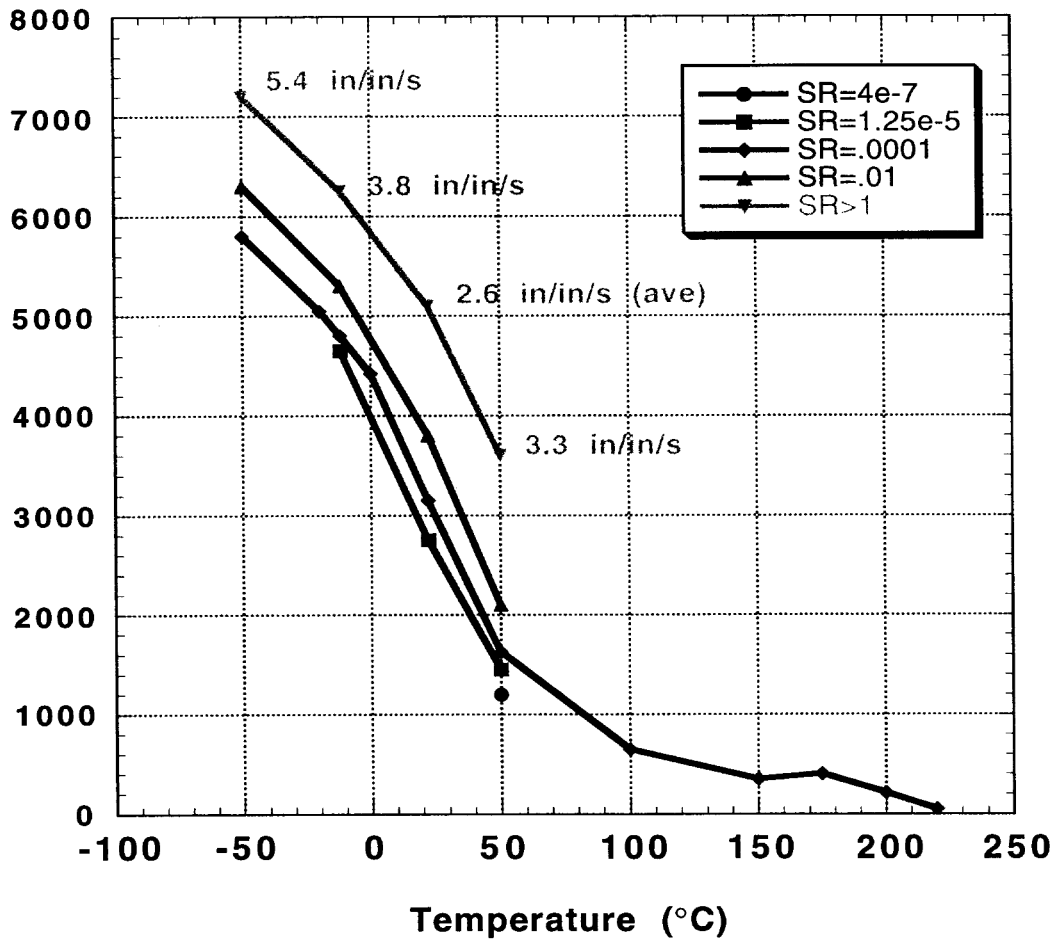


**Figure 28- Straight line fits to the upper portions of strain-time curves for the purpose of determining effective strain rates in high rate tests.**

### LX17-1 Compression - Ultimate Strengths



re 29 – Summary plots of LX17-1 ultimate strengths in compression as a function of temperature and strain rate.

**LX17-1 Compression At High Temperatures  
Strain Rate = .0001 in/in/s**

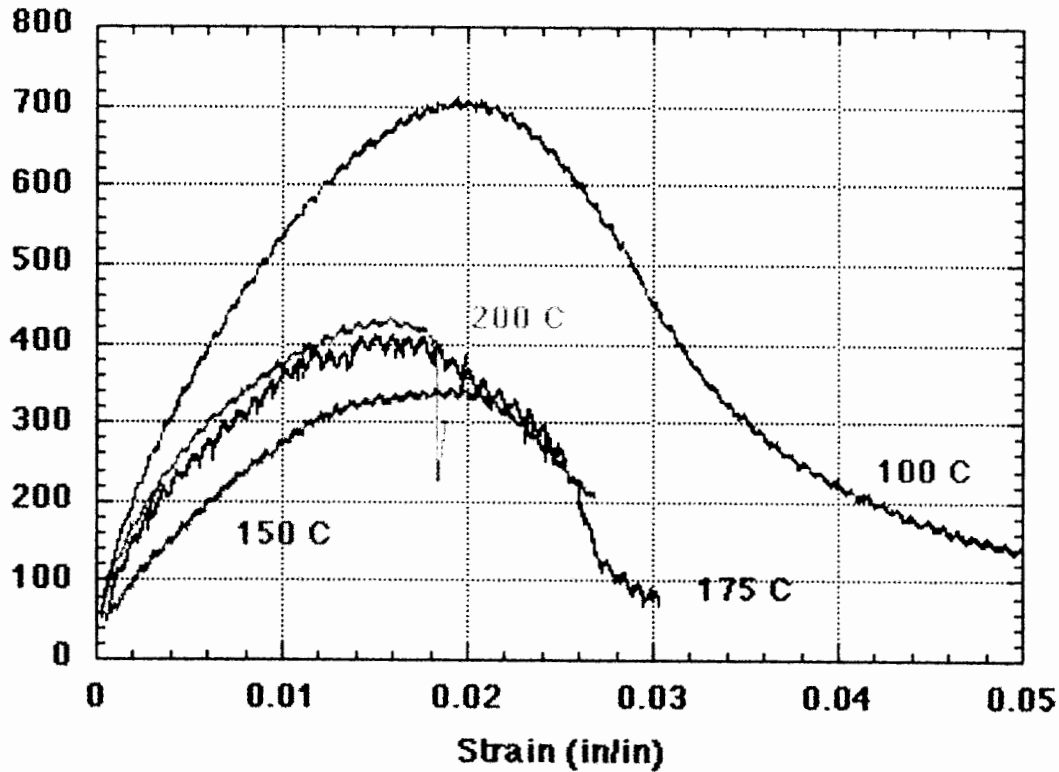


**Figure 30 – High temperature compression data showing somewhat erratic results for LX17-1 in compression at 100° C and above. This is probably due to the fact that the melt point of the binder has been exceeded at these temperatures.**

### LX17-1 Compression - Initial Modulus

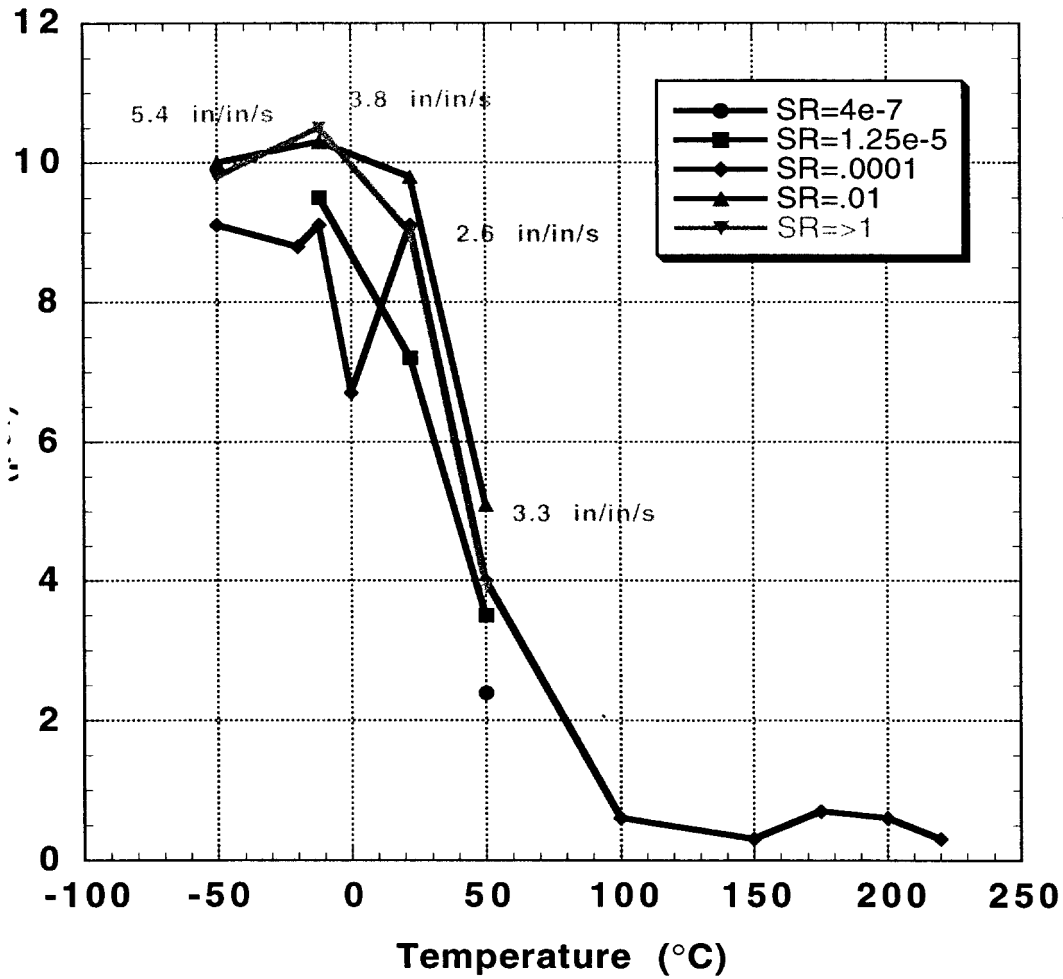
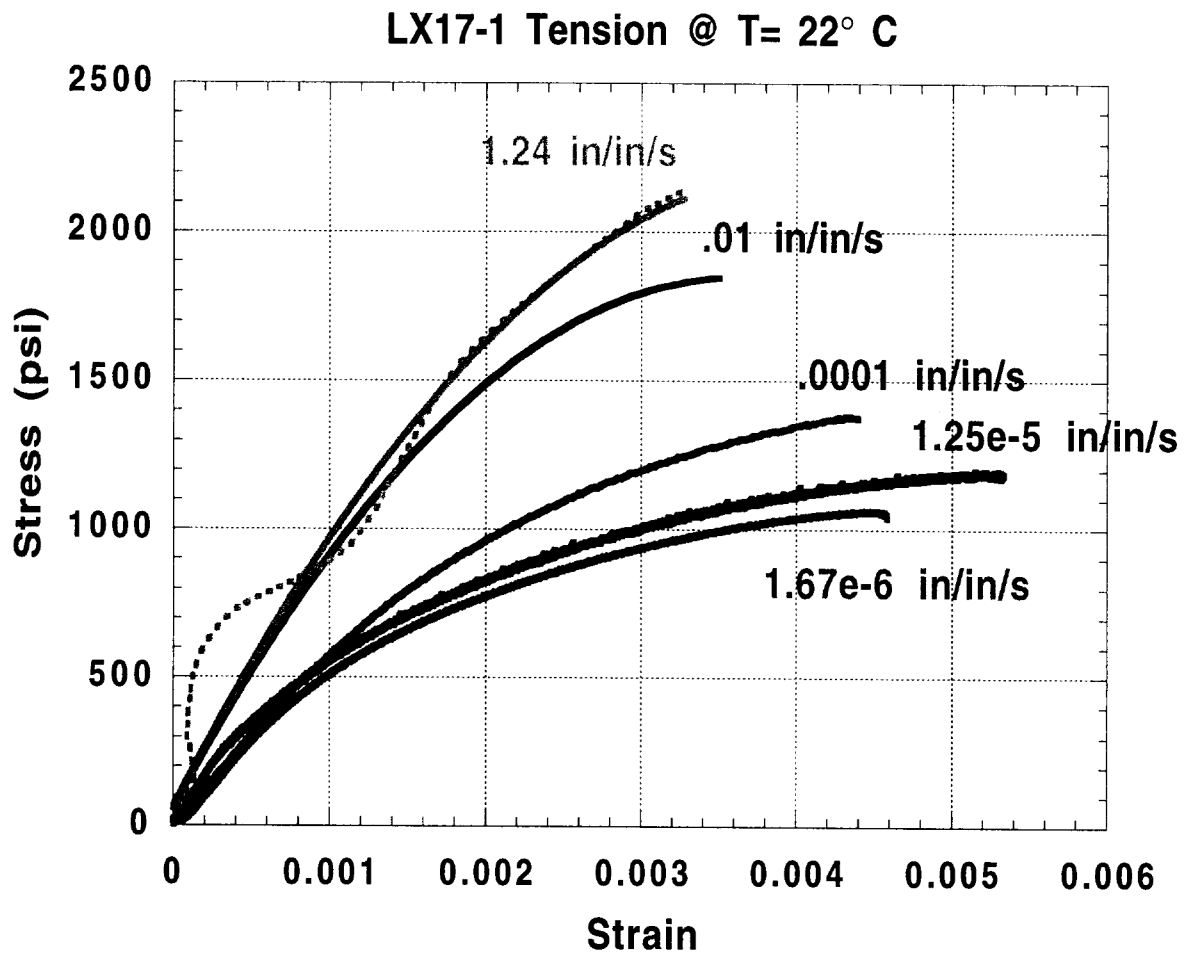
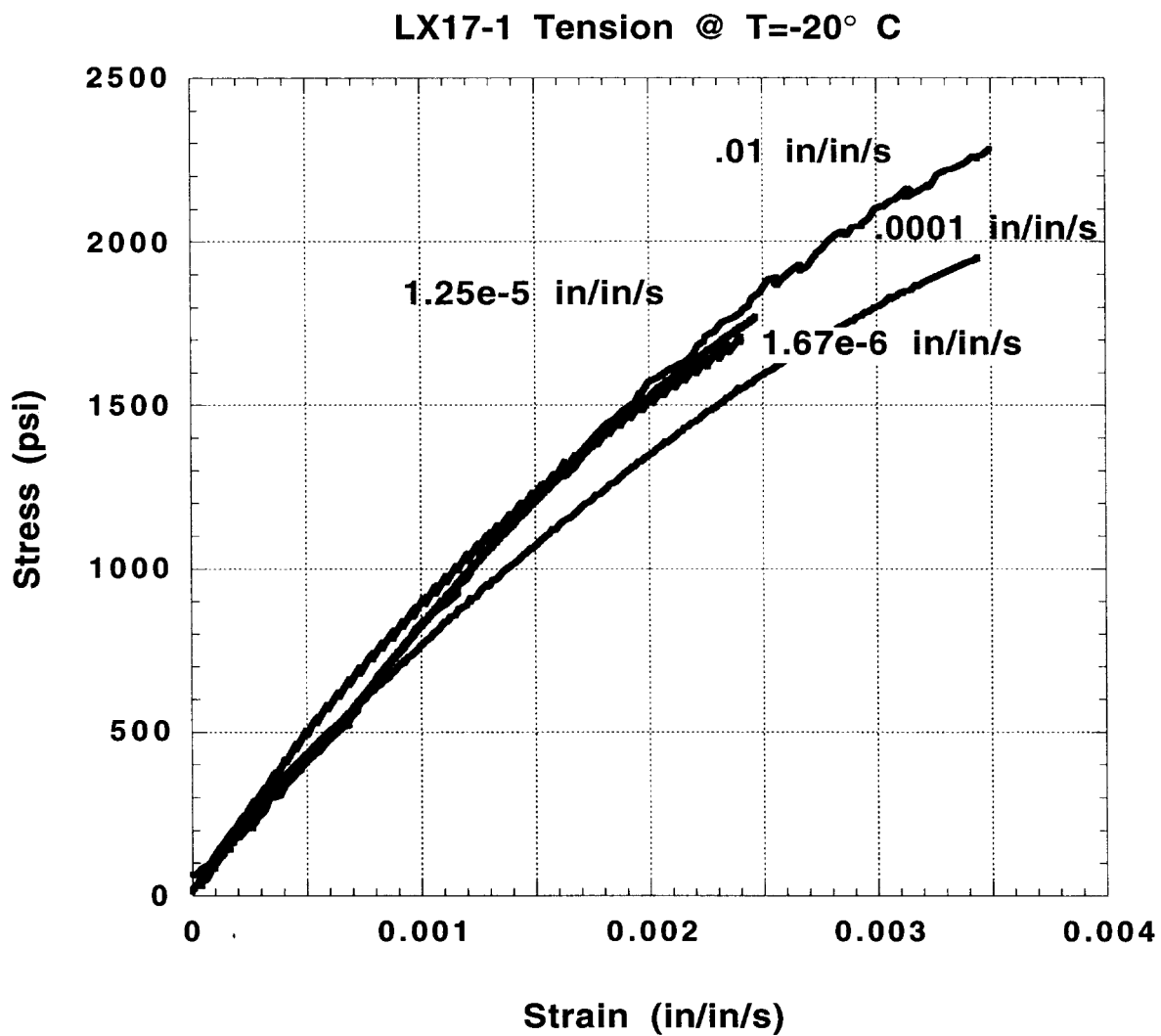


Figure 31 – Summary plots of LX17-1 initial moduli in compression as a function of temperature and strain rate.



**Figure 32 – Stress-strain tensile data at 22° C and five strain rates. The dotted line is the actual high rate data overlaid with a fit to the data (solid line).**



**Figure 33 – Stress-strain data at -20° C and four strain rates. These curves are relatively tightly grouped, but show some lack of ordering in overall modulus at low strain rates.**

LX17-1 Tension @ T=0° C

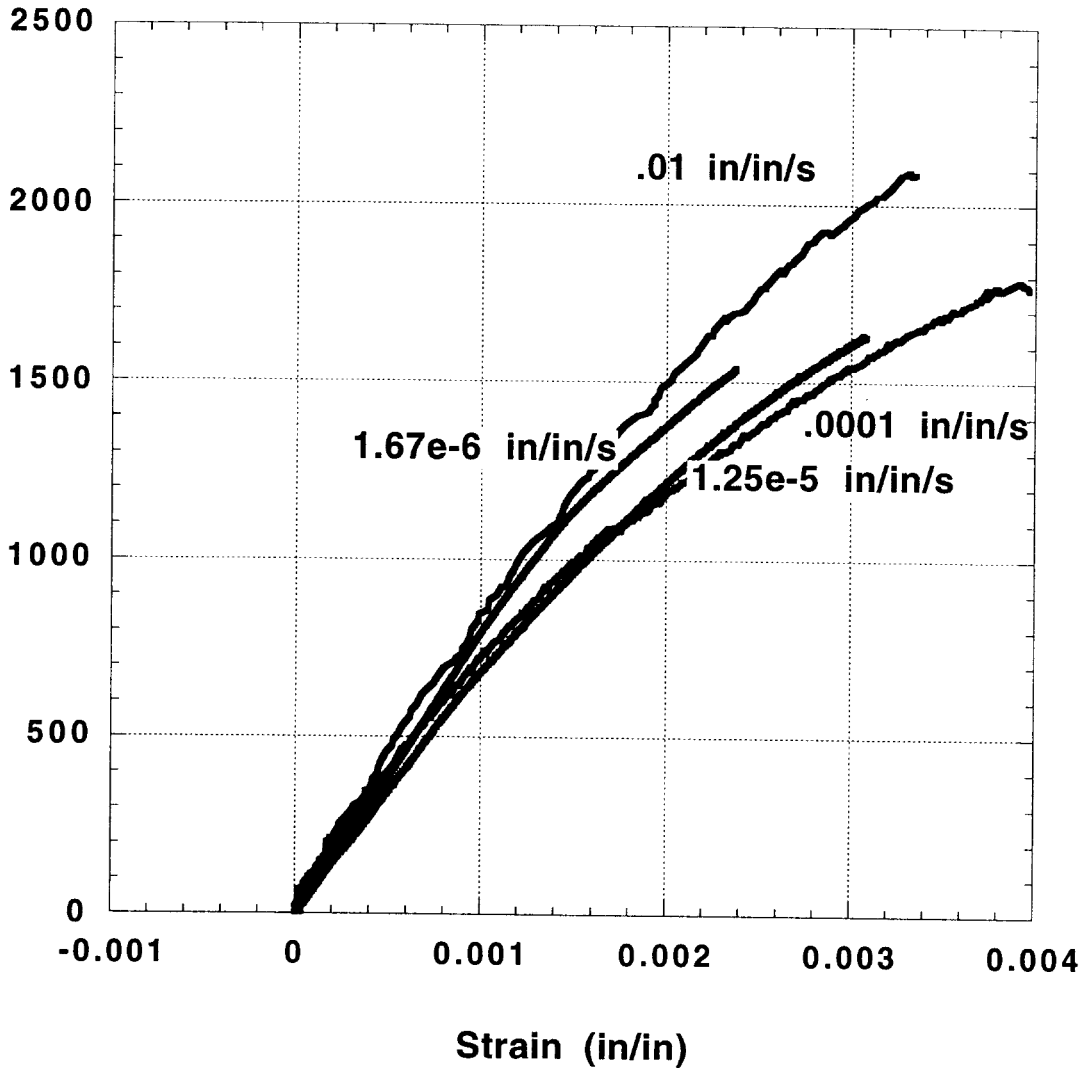


Figure 34 – Stress-strain tensile data at 0° C and four strain rates. As in Figure 33, these curves do not show the expected ordering in overall modulus at the three lowest strain rates. The plots are, however, relatively tightly clustered.

LX17-1 Tension @ T=50° C

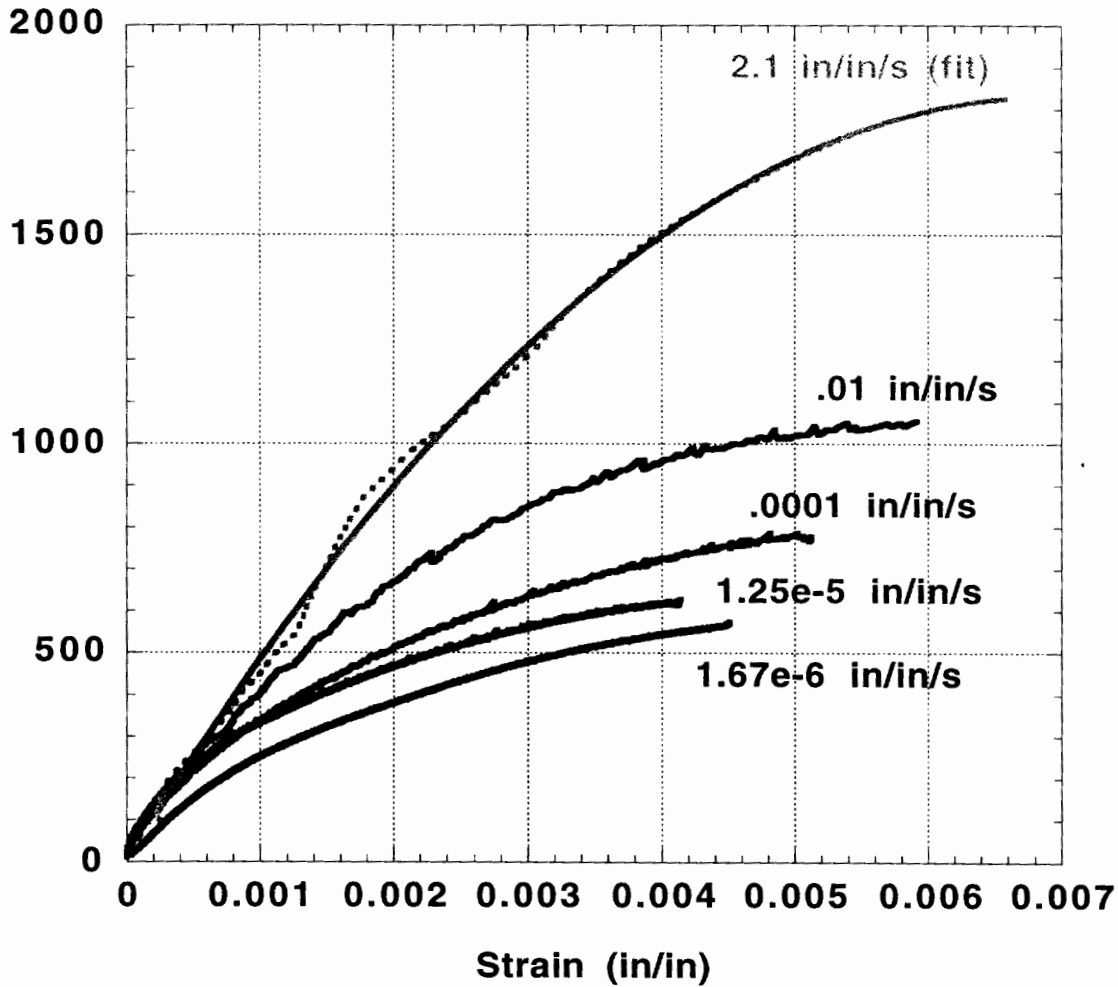


Figure 35 – Stress-strain tensile data at 50° C and five strain rates.

LX17-1 Tension @ SR=.0001 in/in/s

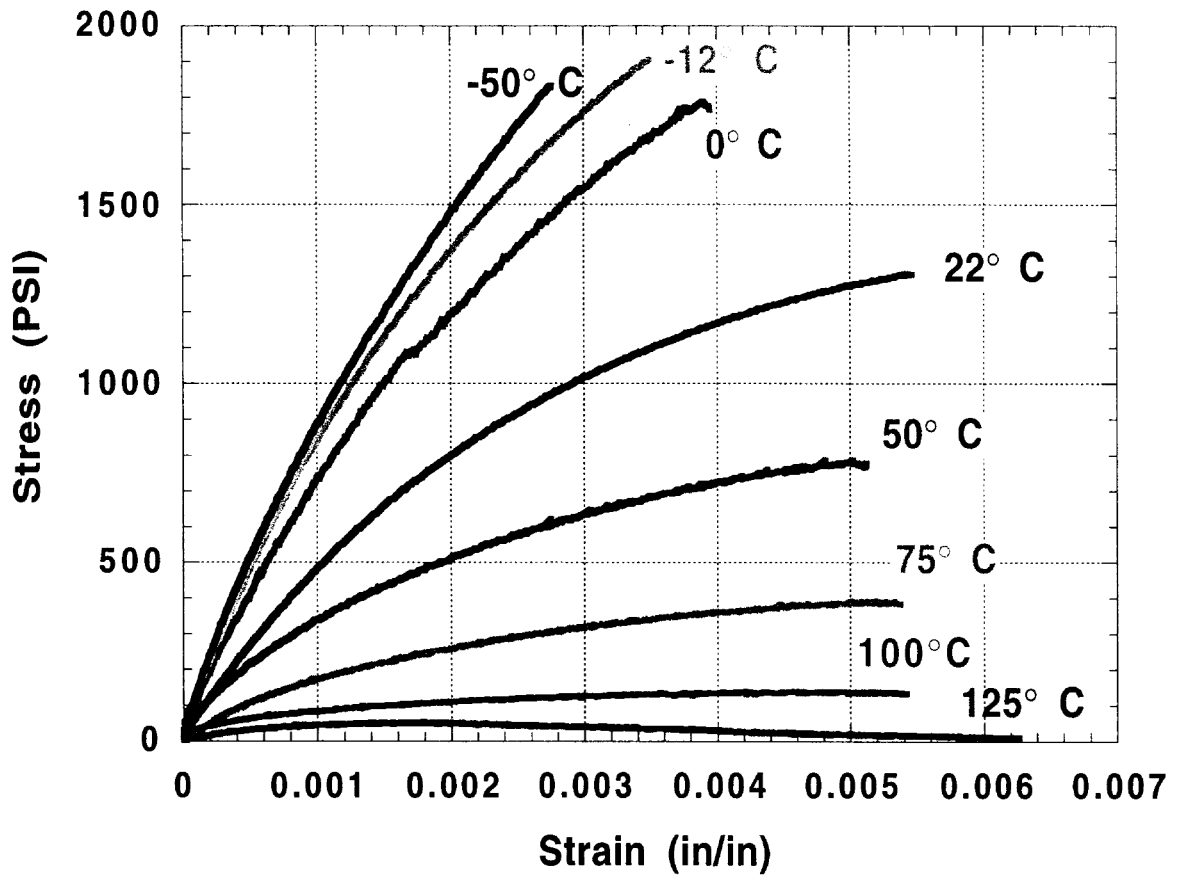


Figure 36 – Stress-strain tensile data at strain rate = .0001 in/in/s and eight temperatures.

LX17-1 Tension @ SR=1.67e-6 in/in/s

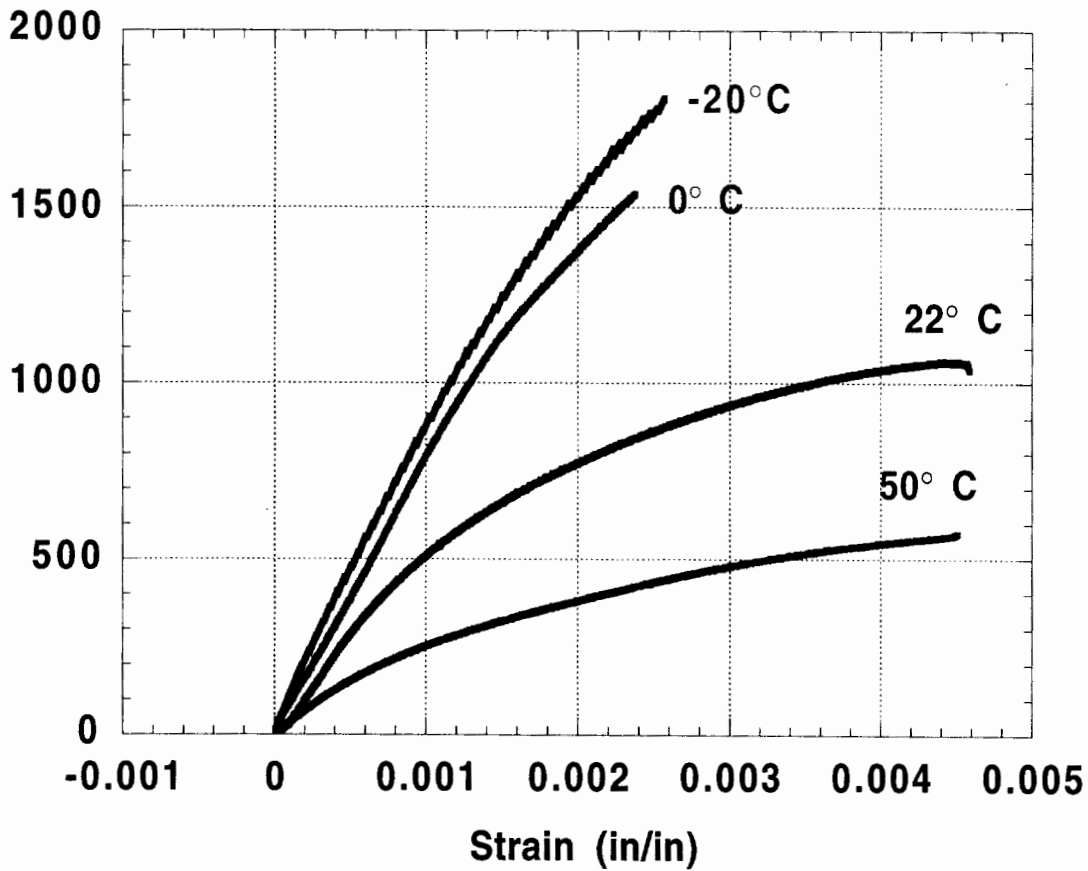


Figure 37 – Stress-strain tensile data at strain rate = 1.67e-6 in/in/s and four temperatures.

LX17-1 Tension @ SR=1.25e-5 in/in/s

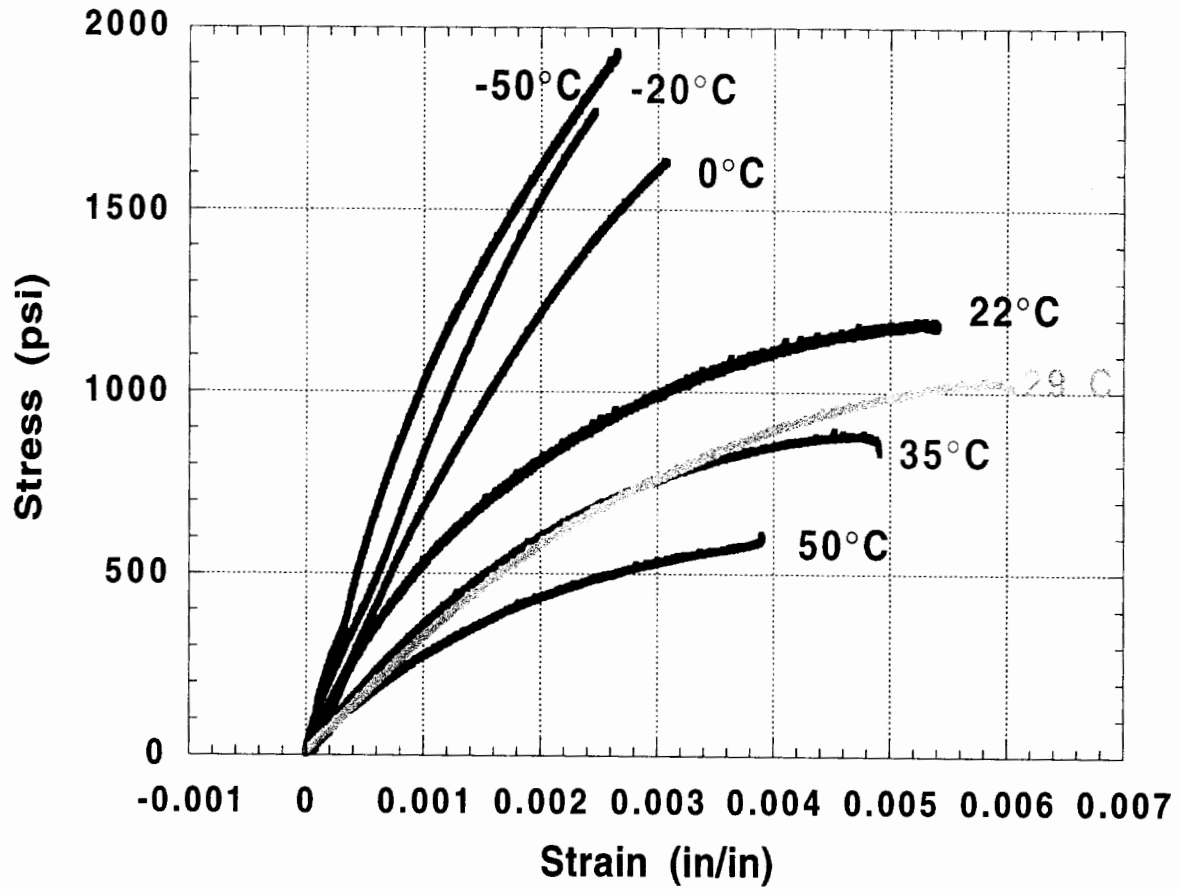
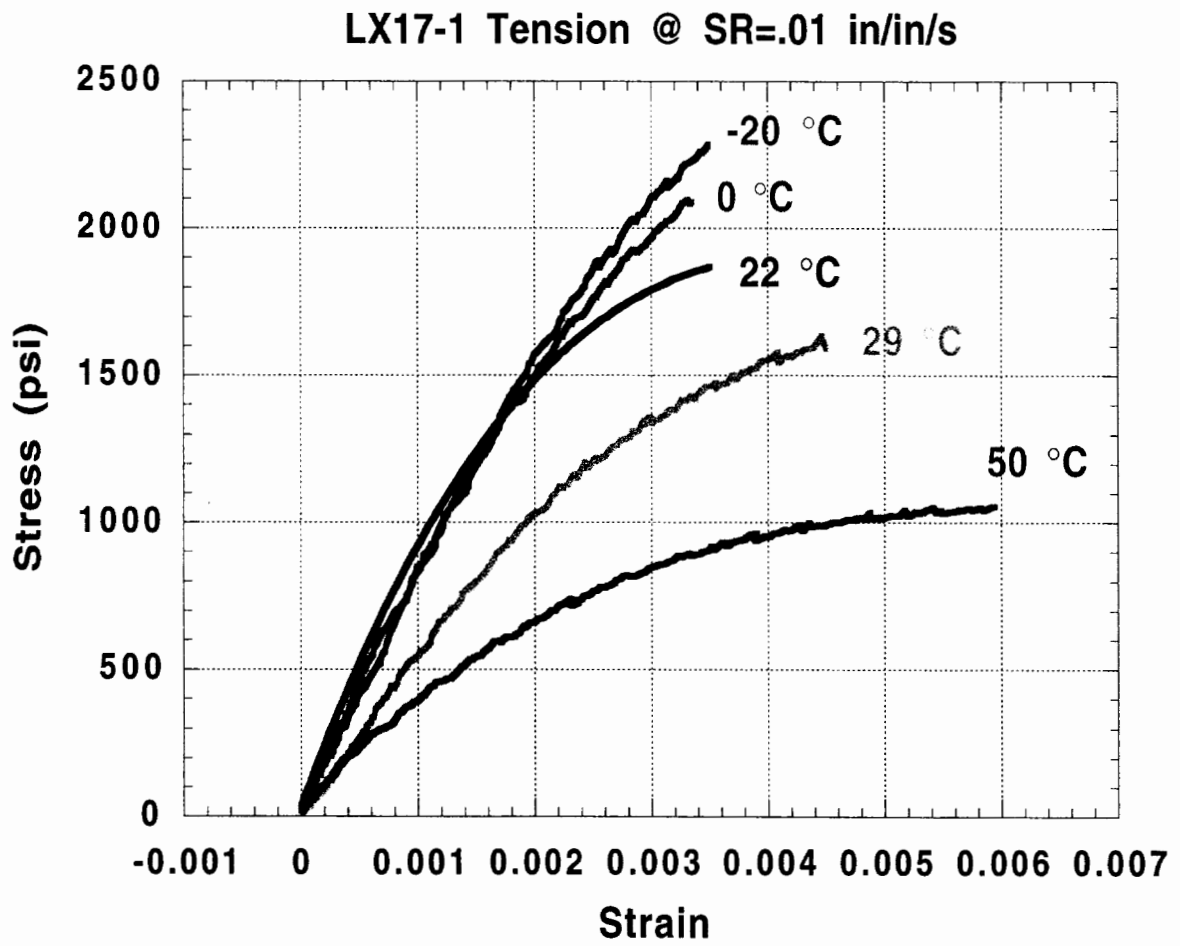
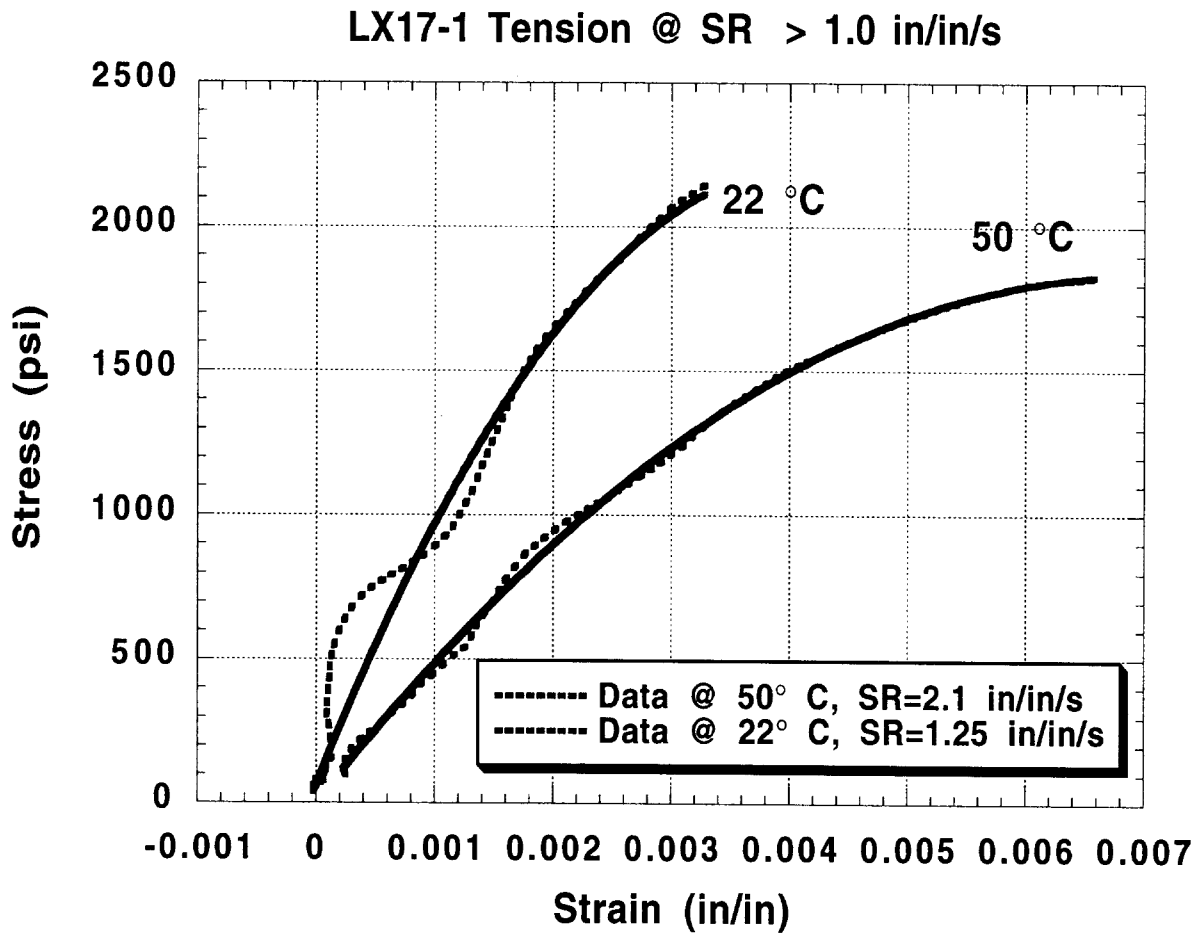


Figure 38 – Stress-strain tensile data at strain rate = 1.25e-5 in/in/s and seven temperatures.



**Figure 39 – Stress-strain tensile data at strain rate = .01 in/in/s and five temperatures.**



**Figure 40 – Stress-strain tensile data at strain rates greater than 1.0 in/in/s and two temperatures.**

### LX17-1 Ultimate Tensile Strengths

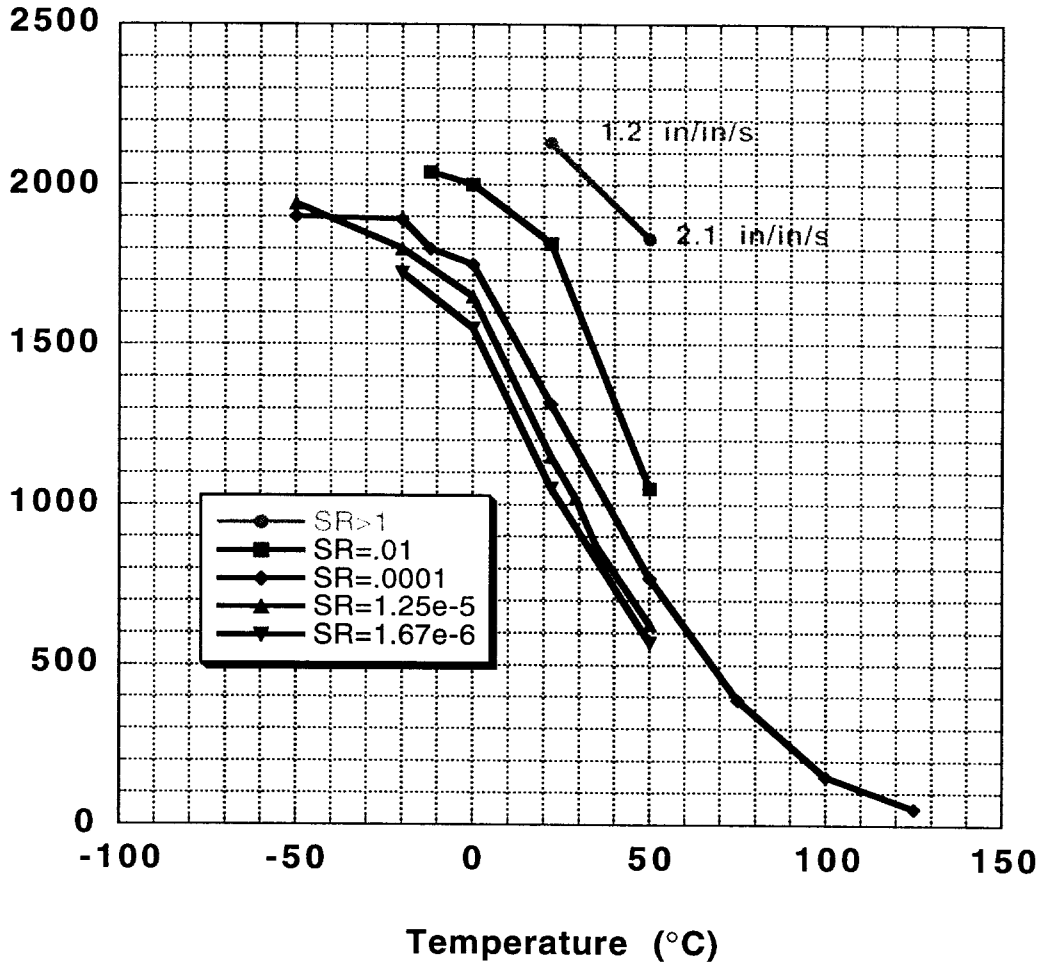
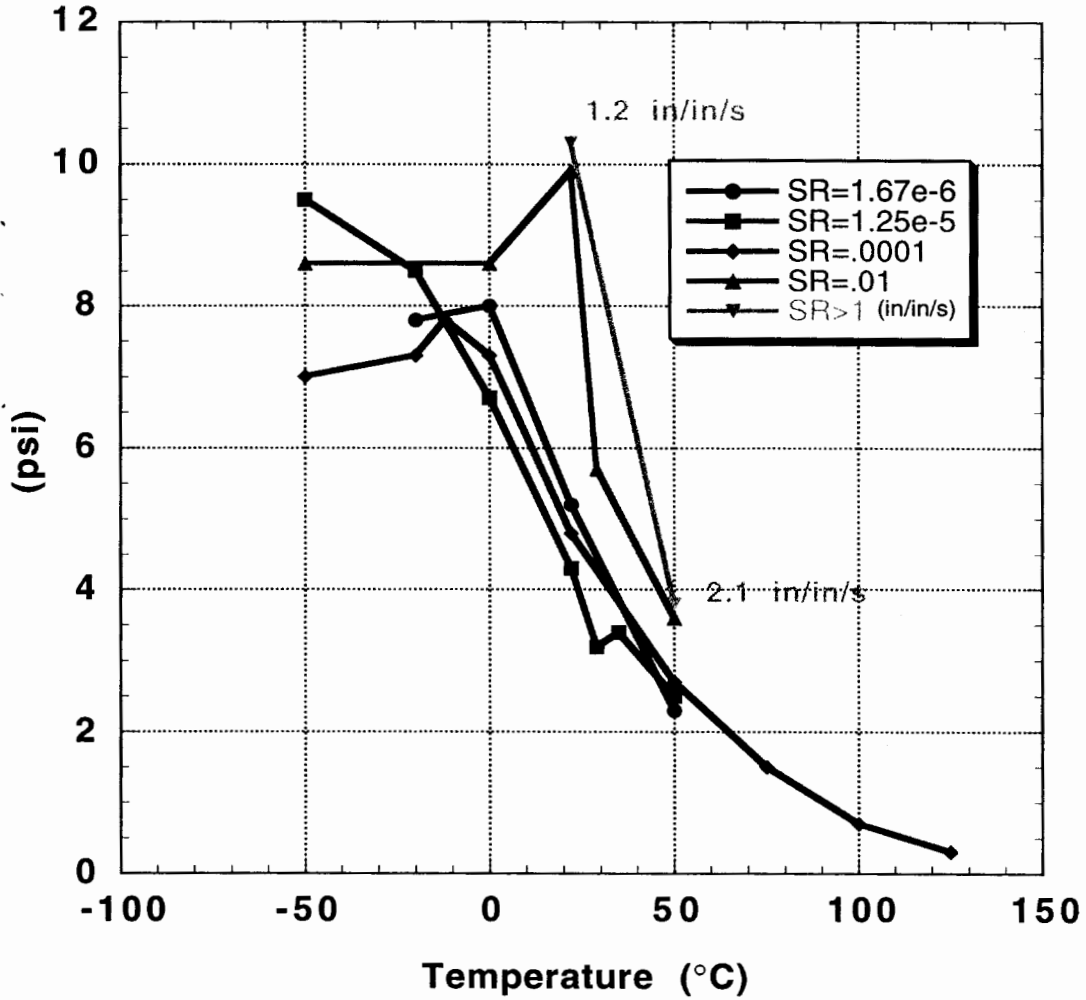


Figure 41 – Summary plots of LX17-1 ultimate tensile strengths as a function of strain rate and temperature.

### LX17-1 Tension - Initial Modulus



re 42 – Summary plots of LX17-1 initial moduli in tension as a function of strain rate and temperature.

### LX17-1 Ultimate Tensile Strains

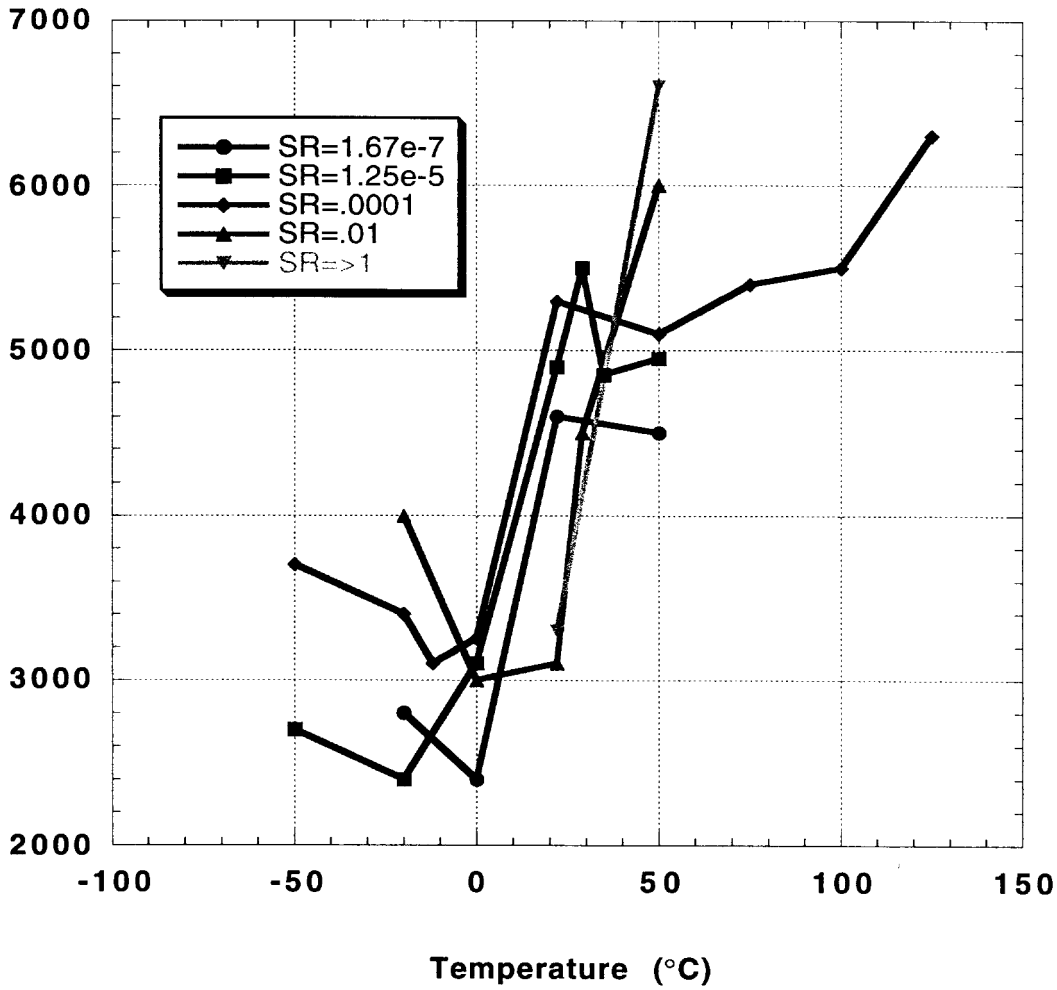


Figure 43 – Summary plots of LX17-1 ultimate tensile strains as a function of strain rate and temperature.